

# A2Z-10M+: Geometric Deep Learning with A-to-Z BRep Annotations for AI-Assisted CAD Modeling and Reverse Engineering

Pritham K. Jena<sup>1,2</sup> Bhavika Baburaj<sup>1,2</sup> Tushar Anand<sup>2</sup> Vedant Dutta<sup>2</sup> Vineeth Ulavala<sup>2</sup>  
Sk Aziz Ali<sup>1,2†</sup>

<sup>1</sup>3D Vision Group (3DVG) <sup>2</sup>BITS Pilani, Hyderabad, India

†Corresponding Author: skaziz.ali@hyderabad.bits-pilani.ac.in

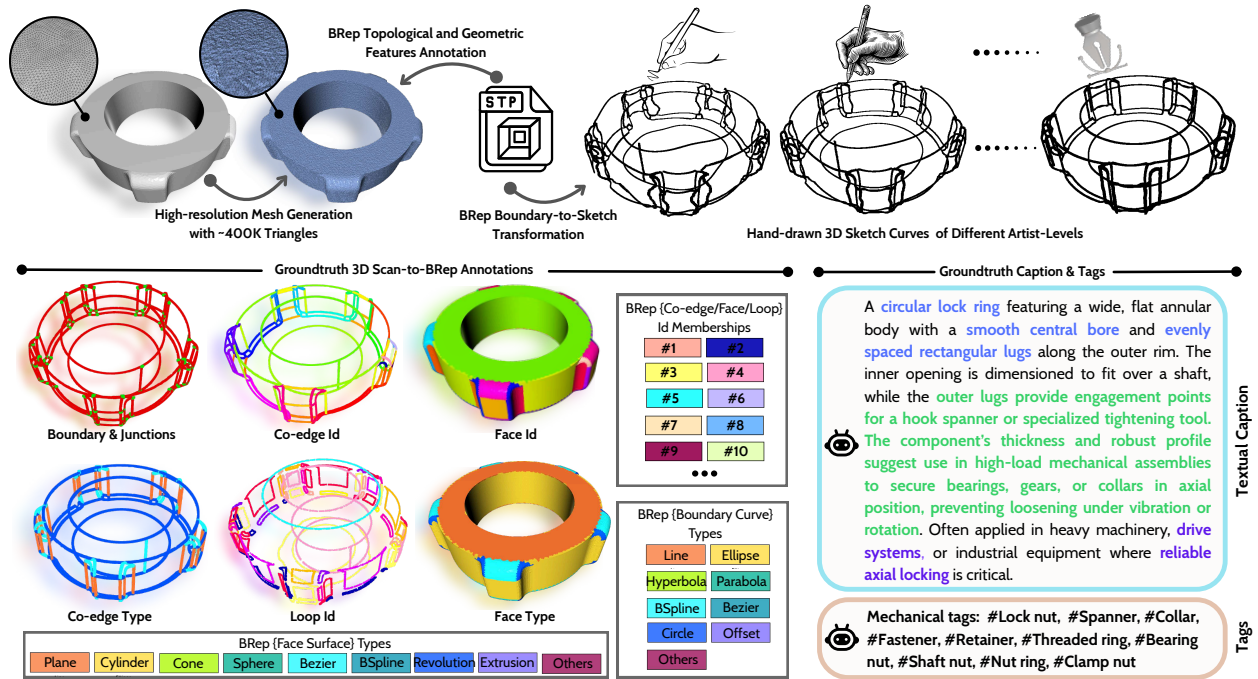


Figure 1. A2Z data and annotations for multi-modal BRep learning in CAD reverse engineering (best viewed when zoomed in).

## Abstract

Reverse engineering and rapid prototyping of computer-aided design (CAD) models from 3D scans, sketches, or simple text prompts is vital in industrial product design. However, recent advances in geometric deep learning techniques lack a multi-modal understanding of parametric CAD features stored in their boundary representation (BRep). This study presents the largest compilation of 10 million multi-modal annotations for 1 million ABC CAD models, namely A2Z, to unlock an unprecedented level of BRep learning. A2Z comprises (i) high-resolution meshes with salient 3D scanning features, (ii) 3D hand-drawn sketches equipped with (iii) geometric and topological information about BRep co-edges, cor-

ners, and surfaces, and (iv) textual captions and tags describing the product in the mechanical world. Creating such carefully structured large-scale data — nearly 5 terabytes of storage — to leverage unparalleled CAD learning/retrieval tasks is very challenging. The scale, quality, and diversity of our multi-modal annotations are assessed using novel metrics, GPT-5, Gemini, and extensive human feedback mechanisms. To this end, we also merge an additional 25K CAD models of electronic enclosures (e.g., tablets, ports) created by skilled designers with our A2Z dataset. Subsequently, we train and benchmark a foundation model on a subset of 300K CAD models to detect BRep co-edges and corner vertices from 3D scans, a key downstream task in CAD reverse engineering. Project page and dataset details are available [here](#).

# 1. Introduction

Geometry processing [3], topological exploration [64], and understanding of design principles [24] are essential components of industrial product design [9, 52] and reverse engineering [2, 60]. In industrial product design and manufacturing, boundary representation (BRep) is the *de facto* standard for feature-based geometry processing and topological exploration of CAD models [31]. As shown in the Fig. 1, a BRep can be seen as a hierarchical structure of geometric primitives where solid shells of a CAD model are composed of surface primitives (e.g., plane, cylinder, cone), each bounded by a closed loop of one or many boundary curves called co-edges (e.g., line, circle, Bspline). Similarly, the co-edges are further connected by junction/corner vertices. These geometric primitives are connected components, and therefore, can be traversed through a topological walk [64] (i.e., shell → faces → closed loops → co-edges → junctions) over the BRep complex chain [18].

While the final version of any CAD model is stored in its BRep structure, its feature-based modeling includes sequential and repetitive design steps – i.e., continuously drawing 2D sketches (e.g., parametric lines, arcs, or other curves) followed by a 3D operation (e.g., extrusion, revolution, fillet, etc.) [67]. These sequential design steps are collectively referred to as the *design history*. In recent times, the most popular supervised deep learning methods for CAD reverse engineering require high-quality 3D scans paired either with their *design history* [27, 46, 60, 67] or precisely annotated BRep information [2, 8, 18, 43, 53, 61] for robust training.

Obtaining the design history of all CAD models under ABC [30] requires proprietary access to the OnShape [1] repository, which is non-permissive. At the same time, generating high-quality 3D scans from *one million* low-poly meshes of ABC has never been done before<sup>1</sup>. Therefore, all *design history*-based CAD construction methods depend upon ~170K CAD samples from the DeepCAD [67] dataset. However, this dataset primarily comprises rudimentary CAD models, with the majority of shapes being *simple* cuboid type, exhibiting minimal diversity in terms of geometry, topology, and shape categories. The main reason behind this is the selection of only those CAD models that are designed through simple extrusion operations on easily drawn 2D sketches. Furthermore, the input point clouds employed by methods like MultiCAD [46], DeepCAD [67], CAD-SIGNet [27], and Point2Cyl [60] consist of randomly subsampled points from the clean BRep face patches of

<sup>1</sup>traditional NeRF is not an alternative to the 3D scanning process and we cannot manufacture [29] a NeRF.

Dataset	CAD Models	#Models	BRep Labels	Text Caption	3D Scans	3D Sketch	Design History
DeepCAD [67]	Simple ✓	170,000+	✗	✗	✗	✗	✓
Fusion360 [65]	Simple ✓	~8,000	✗	✗	✗	✗	✓
CADParser [73]	Simple ✓	41,000	✗	✗	✗	✗	✓
CAD-MLLM	Simple ✓	453,220	✗	✓	✗	✗	✓
ABC [30]	Cmplx. ✓	1,000,000	✗	✗	✗	✗	✗
CC3D-Ops [13]	Cmplx. ✓	~50,000	✓	✗	✓	✗	✗
ABCPrimitive [21]	Simple ✓	5,619	✓	✗	✗	✗	✗
<b>A2Z (Ours)</b>	Cmplx. ✓	1,025,000+	✓	✓	✓	✓	✗

Table 1. Comparison of open-source CAD datasets w.r.t **A2Z**

CAD models. This is because of the unavailability of real scans as highlighted in [47]. In summary, this is a deadlock situation for design history-based CAD modeling methods to advance. The other group of BRep-based CAD reconstruction methods from input point clouds [2, 8, 18, 43, 53] uses either the Fusion-360 Gallery data [65] with 8K samples or the ABCParts [53] dataset, which is a small subset of just 32K samples from ABC [30]. Though the BRep information is available in the *.step* file of a CAD model, the corresponding high-quality 3D scans and annotations are not available.

The previously mentioned scarcity of large-scale data and the lack of rich multi-modal annotations remain major obstacles in advancing CAD reverse engineering research. These limitations also restrict research progress in BRep reconstruction, developing novel approaches like freehand 3D sketch-to-BRep generation, text-to-BRep modeling, and other broader semantic reasoning tasks for *complex* CAD models. As a result, existing methods for BRep parsing and fitting – like BRepSeg [15], ParseNet [53], HPNet [70], SPFN [40], its extension CPFN [14], and ComplexGen [18] – are not robust enough (reasons are highlighted in Sec. 2). To overcome these data challenges and leverage many new avenues of multi-modal BRep learning, we derive A2Z as the largest compilation of >10 million annotations for >1 million complex CAD models. In Tab. 1, we elaborate on different open-access datasets and their multi-modal annotations compared to our **A2Z**. This illustrates the present importance and further impact our proposed A2Z dataset can make in advancing supervised X-to-BRep representation [22, 31] learning. Our main **contributions** are:

**3D Scans with BRep Labels.** We process 1 million low-poly CAD meshes of ABC and upscale them into 16x higher resolution meshes. Each vertex is labeled by its corresponding BRep co-edge, junction, and face information using a proximity-aware, multi-threshold assignment policy (see Sec. 3.2). We also propose a geometric transformation algorithm that imprints natural

artifacts observed in real 3D scans [7, 47] – e.g., surface dents, missing parts, protrusions near small holes, and surface roughness (see Sec. 3.1). The resulting **A2Z** is the largest dataset for scan-to-CAD reverse engineering.

**Multi-Level 3D Sketching:** We generate 3D sketches using a novel algorithm that simulates different skill levels of drawing artists. Using normalized arc-length parameterization of BRep co-edge curves, we induce realistic deformation [17], distortion, intentional endpoint openings, planar tapering [19], and other haptic sketching traits [66] (see Sec. 3.3).

**Vision-Language Models (VLMs) for Captions.** A2Z is the first to automate high-quality captions ( $\leq 200$  words per model) and tags ( $\leq 20$  per model) for the entire ABC corpus using a cost-effective VLM system (see Sec. 3.4). Inspired by ImageNet [12] and WordNet [16], we also derive a hierarchical class and category structure (with a depth of up to 4) based on a key ontology.

**Additional CAD of Electronic Enclosures.** We employ skilled designers to create 25K CAD models of electronic enclosures – e.g., charging ports, thin casings, and sockets – on OnShape [1]. These models, with annotations, are merged into A2Z (see Sec. 3.5).

**Benchmarking A2Z.** Finally, we train and benchmark a geometric deep learning model for BRep boundary and junction detection tasks (see Sec. 4 and Sec. 5.2). Data analytics, human feedback scores of A2Z multi-modal annotations, and comparisons with Gemini [58] and GPT-5 [50] are systematically staged (see Sec. 5.1).

## 2. Related Work

### 2.1. Supervised Scan-to-BRep Learning

Many recent methods for B-Rep learning [2, 18, 41, 43] follow a common pipeline. They first estimate junction and boundary vertices from an input point cloud and learn edges-to-corners connectivity to form a topological graph, yielding a CAD wireframe. PIE-Net [62], BRepDetNet [2], and ComplexGen [18] focus on boundary and corner detection as the initial challenges in BRep learning. Conversely, ParseNet [73], BGPSeg [15], SPFN [40], and CPFN [14] perform BRep surface segmentation as their primary task for CAD construction. Only Point2CAD [43] and ComplexGen [18] advance to parametric surface fitting. However, estimating adjacency [35, 39, 42] through point membership assignment into boundaries, corners, loops, and faces is never jointly addressed, mainly due to the absence of exhaustive BRep labels in public datasets (see Tab. 1).

### 2.2. Multi-modal Annotations for CAD

Recent years have seen a rapid rise in publicly available BRep datasets [7, 22, 30, 33, 44, 65]. However, except for CC3D [7, 47], most datasets contain synthetic CAD

models (in ‘.step’ file format) without paired 3D scans. For instance, MFCAD [33], FabWave [56], SolidLetters [22], Fusion-360 [65], and ABC [30] are all synthetic CAD models designed on the Fusion-360 API [4] or Onshape [1] platform. Although BRep information parsing from these datasets is feasible, there remains a lack of consistent class-level annotations, 2D/3D free-form sketches, realistic 3D scans, multi-view images (2D), and textual captions or tags (1D). For example, state-of-the-art generative BRep methods like SolidGen [23] and BRepGen [69] use the DeepCAD dataset and partially selected ( $<90K$ ) CAD models of ABC. Meanwhile, other BRep modeling methods exploiting synthetically rounded boundaries [32], smooth fillets [25], or sharp boundaries [48] rely on varied workarounds across datasets. Although many datasets exist for 3D content generation from text [38], sequential CAD design steps from sketches [36, 37], or text inputs [28], none provide large-scale, unified, and multi-modal annotations. Only HoLABRep [44] has aligned ABCPrimitive [21] with textual and basic sketch annotations.

## 3. A2Z Data and Annotation Processing

We treat a boundary representation (BRep)  $\mathcal{B}$  of a CAD model as a chain complex  $\mathcal{C} = (\mathcal{V}, \mathcal{E}, \mathcal{F}, \mathcal{A})$  where the set of faces  $\mathcal{F} \in \mathbb{R}^{n_f \times 1}$  is defined by their ids and stores surface parameters along with other features, co-edges  $\mathcal{E} \in \mathbb{R}^{n_e \times 1}$  are defined by their ids and store likewise parametric curve features, and corner vertices  $\mathcal{V} \in \mathbb{R}^{n_v \times 1}$  are defined by their ids along with Euclidean coordinates (see Fig. 1). Therefore, the 2D adjacency matrices  $EV \in \{0, 1\}^{n_e \times n_v}$  and  $FE \in \{0, 1\}^{n_f \times n_e}$  can determine the edges-to-corners and faces-to-edges topological connectivity. In addition, the topological walk along the co-edges is also expressed by the matrix  $\mathcal{A}$  as a tuple of three transition vectors  $(\mathcal{N}, \mathcal{P}, \mathcal{M}) \in \mathbb{R}^{n_e \times 1}$ , namely next, parent, and mate. For instance, to know the *the mating face id of another face that is next to my current co-edge id e*, we can express the topological walk as  $\mathcal{F}[\mathcal{M}[\mathcal{N}[\mathcal{E}[e]]]]$  (see [22]). During the annotation process, we transfer the true IDs, topological connections, and geometric features of  $\mathcal{B}$  to every vertex  $\mathbf{p}_i$  of its paired 3D scan  $\mathcal{P} = \{\mathbf{p}_i\}_{i=1}^N$  that corresponds to either  $\mathcal{V}$ ,  $\mathcal{E}$ , or  $\mathcal{F}$ . BRep primitives like loops  $\mathcal{L}$  can also be derived as the chord-free cycles of edges  $\in \mathcal{E}$ , or shells can be as a closed volume of faces  $\in \mathcal{F}$ .

### 3.1. High Resolution Meshes like 3D Scans

We begin with a low-polygon triangular mesh  $\mathcal{M}^{\text{init}} = (\mathcal{V}^{\text{init}}, \mathcal{T}^{\text{init}})$  sourced from the ABC dataset, together with its corresponding BRep  $\mathcal{B}$ . Our main objective is to transform  $\mathcal{M}^{\text{init}}$  into a high-resolution, scan-like mesh  $\mathcal{M}$  that accurately reflects the imperfections, occlusions, noisy surface perturbations, protrusions, and cavi-

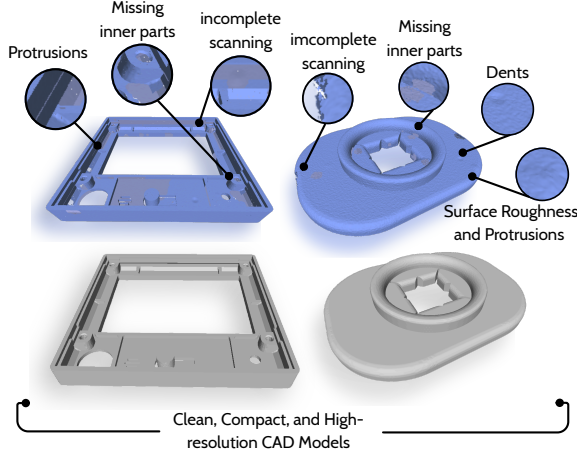


Figure 2. Low-poly CAD meshes are compared to high-quality scans after a series of geometry processing steps (Sec. 3.1).

ties commonly observed in data acquired by short-range handheld scanners, e.g., Artec3D (artec3d.com) or Scantech devices. These transformations are carried out through a sequence of geometry processing steps.

**Step-I: Mesh Upsampling.** We apply two successive iterations of midpoint subdivision of triangles in  $\mathcal{M}^{init}$ . This results in a refined mesh  $\mathcal{M} = (\mathcal{V}, \mathcal{T})$  with approximately  $1.5 \times 10^5$  vertices and  $3.8 \times 10^5$  triangles, a density comparable to meshes reconstructed from high-precision scanning systems. Therefore, the vertices  $\mathcal{V}$  are now equivalent to  $\mathcal{P}$ . To apply the transformations, we dense sample vertices  $\mathbf{x}$  on the parametric uv-grid [22] of  $\mathcal{F}$ , arc-length  $\mathcal{E}$ , and corners  $\mathcal{V}$  of  $\mathcal{B}$ .

**Step-II: Tangential Shrinkage Near Small Loops.** To replicate realistic scan imperfections, we first identify small loops in  $\mathcal{B}$ . For each loop  $\ell \in \mathcal{L}$ , its perimeter  $L_\ell$  is compared against the maximum  $L_{\max} = \max_{\ell \in \mathcal{L}} L_\ell$ . The loops with  $L_\ell/L_{\max} < \tau_h$  (given  $|\mathcal{L}| > 2$ ) are classified as tiny holes  $\mathcal{H}$ . Such small openings are prone to poor capture due to sensor frustum limitations (see Fig. 2). To mimic this effect, vertices adjacent to  $\ell \in \mathcal{H}$  are shrunk tangentially toward the loop centroid  $\mathbf{c}_\ell$  using the in-plane projector  $P_\ell = I - \mathbf{n}_\ell \mathbf{n}_\ell^\top$ :

$$\Delta \mathbf{x}_{\text{shrink}} = \mathbf{x} - \eta_\ell w_\ell(\mathbf{x}) P_\ell(\mathbf{x} - \mathbf{c}_\ell),$$

thereby introducing protrusions and small gaps that simulate visibility loss. In addition, incomplete coverage is reinforced by removing a controlled subset of triangles from the mate-face  $f_{\text{mate}}(\ell) \in \mathcal{F}$ , subject to

$$\sum_{t \in \mathcal{T}_{\text{miss}}(\ell)} \text{Area}(t) \leq 0.2 \text{Area}(f_{\text{mate}}(\ell)),$$

which models the occlusion of regions lying behind narrow openings.

**Step-III: Adding Surface Roughness.** Real-world scanned surfaces exhibit both measurement error and small irregularities. We emulate this by displacing each vertex  $\mathbf{x}$  along its normal  $\mathbf{n}(\mathbf{x})$  using a multi-octave Perlin noise [51] field  $N : \mathbb{R}^3 \rightarrow [-1, 1]$ :

$$\Delta \mathbf{x}_{\text{rough}} = A_r \sum_{o=1}^O \lambda_o N(\omega_o \mathbf{x}) \mathbf{n}(\mathbf{x}),$$

with  $\sum_o \lambda_o = 1$  and  $\omega_o$  as increasing scalar field across octaves  $O$ . This step injects millimeter-scale inaccuracies while preserving sharp edges.

**Step-IV: Adding Dents and Protrusions.** In the final step, to capture manufacturing artifacts, we randomly select planar B-Rep faces and define  $K$  seed points  $\{\mathbf{s}_k\}_{k=1}^K$ . Around each seed, we introduce localized circular dents and subtle bumps based on the outward or inward direction of the seed point’s normal vector:

$$\Delta \mathbf{x}_{\text{dent|bump}} = \sum_{k=1}^K \left( -\delta_k e^{-\frac{\|P_f(\mathbf{x} - \mathbf{s}_k)\|_2^2}{2\rho_k^2}} + \varepsilon_k \sin \frac{\pi \|P_f(\mathbf{x} - \mathbf{s}_k)\|_2}{\rho_k} \right) \times \mathbf{n}(\mathbf{x}).$$

where  $P_f$  projects onto the face plane,  $\delta_k$  sets dent depth,  $\rho_k$  the affected radius, and  $\varepsilon_k$  the amplitude of protrusion or bump (see Fig. 2).

### 3.2. Proximity-Aware Smooth Annotations

We replace the most commonly practiced hard nearest-neighbor rule with a novel policy of multiscale, BRep coedge length-aware, and SPH-weighted [49] membership assignment<sup>2</sup> Given the 3D scan points  $\mathcal{P} = \{\mathbf{p}_i\}_{i=1}^N$  from the high-quality mesh, we use the sampled points  $\mathbf{x}$  on  $\mathcal{B}$  that have already gone through the transformation steps described in Sec. 3.1, i.e.,

$$\mathbf{x} \mapsto \mathbf{x} + \Delta \mathbf{x}_{\text{shrink}} + \Delta \mathbf{x}_{\text{rough}} + \Delta \mathbf{x}_{\text{dent|bump}} \quad (1)$$

and define a local frame around  $\mathbf{x}$ . Next, the SPH weights  $W_k^{\text{spH}}$  are aggregated across different neighborhoods  $\mathcal{N}(\mathbf{x})$  of  $\mathbf{x}$  at  $K$  different scales as

$$\omega_i(\mathbf{x}) = \sum_{k=1}^K w_k W_k^{\text{spH}}(\mathbf{x}) \quad (2)$$

and choose the probabilistic soft labels  $\pi(\mathbf{x})$ , that *does not* miss nearby candidates, defined by

$$p_i(\mathbf{x}) = \frac{\omega_i(\mathbf{x})}{\sum_{j \in \mathcal{N}(\mathbf{x})} \omega_j(\mathbf{x})}, \quad \pi(\mathbf{x}) = \arg \max_{i \in \mathcal{N}(\mathbf{x})} p_i(\mathbf{x}),$$

for a given scan point  $\mathbf{p}_i$ .

**Boundary annotations:** Each vertex  $\mathbf{p}_i$  that is labeled as a boundary now stores the parent edge id  $e$  in  $\mathcal{E}$ , its corresponding loop id  $\ell$  in  $\mathcal{L}$ , the mate loop id  $\mathcal{L}[\mathcal{M}[\mathcal{E}[e]]]$ , the two incident faces in  $\mathcal{F}$ , and a feature vector of the curve primitive (line, circle, spline). Extra scalar fields are reserved for future use.

<sup>2</sup>Detailed formulations are in the supplement.

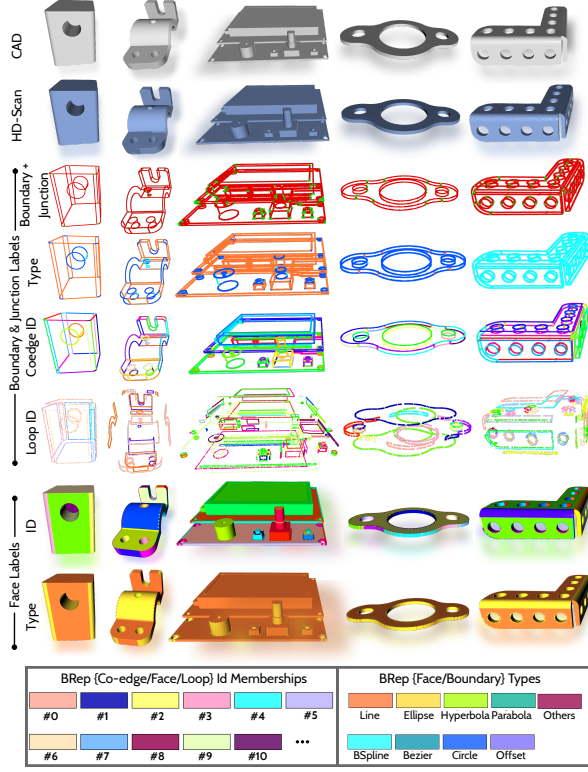


Figure 3. BRep annotations on 3D scans of **A2Z** dataset.

**Junction annotations:** For every junction (*i.e.*, co-edge endpoint), we record the scan–vertex indices as per the soft-label assignment together with the ids of the adjacent loops, edges, and faces.

**Face annotations:** Each scan vertex  $p_i$  is assigned to the closest face in  $\mathcal{F}$  by projection, along with a surface-class code (plane, cylinder, sphere, etc.).

Fig. 3 shows how this concise annotation space fuses topology and geometry, offering rich supervision for deep learning tasks such as boundary detection, loop reasoning, edge typing, and face classification in Scan-to-BRep pipelines. The quantitative data analytics in Fig. 4 illustrate how the distribution of different numbers of CAD models varies when sampled across different areas, face types, co-edge lengths, and types of faces/edges. The top right semivariogram [10] plot in Fig. 4 explains the spatial structure of our high-quality scans  $\mathcal{P}$  w.r.t a normalized separation distance between a group of points from any randomly selected centroid.

### 3.3. 3D Hand-Drawn Sketches of BRep

To generate a 3D sketch from the co-edges  $\mathcal{E} \in \mathcal{B}$ , we apply three different types of displacement fields  $\Delta \vec{u}_{\text{line}}(s)$ ,  $\Delta \vec{u}_{\text{arc}}(s)$ ,  $\Delta \vec{u}_{\text{gen}}(s)$  on the segments  $s$  for three different types of curves – namely, lines, circles/arcs, and all other types of curves grouped in *gen-*

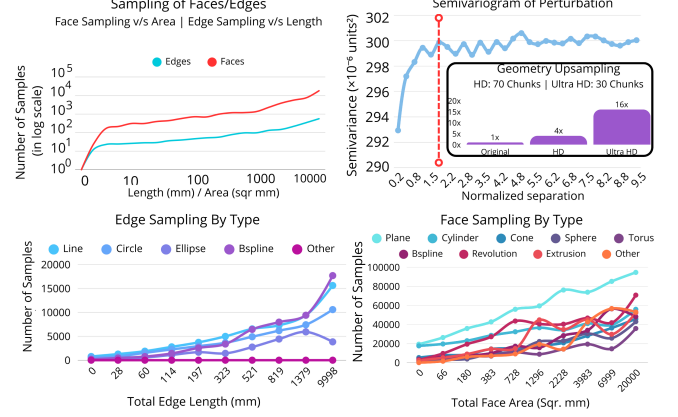


Figure 4. Data and annotation analytics of **A2Z**

*eral* category. First, a local PCA frame [54] is derived on the curve segments  $s$  using their arc-length parameterization. Next, the magnitude of displacement fields is dependent on a single input skill parameter  $\kappa$  defining five different levels (L1 – L5) of sketch artist – *e.g.*, hand drawing level to professional artist. (see Fig. 5 and more results in the supplement).

**Local planar frame.** For each BRep edge  $e \in \mathcal{E}$  with a set of vertices  $\{x_i\}_{i=1}^N$ , its local PCA frame  $\{e_0, e_1, e_2\}$  has the origin  $o = \frac{1}{N} \sum_i x_i$ . The axis  $e_0$  aligns with the principal direction of the edge (tangent). Any point on the edge is mapped to the local 2D coordinates  $(t = e_0^\top(x - o), u = e_1^\top(x - o))$  that are distorted in this flat  $(t, u)$  domain by  $\tilde{x} = o + (t + \Delta t)e_0 + (u + \Delta u)e_1$  (or by polar updates  $\Delta r, \Delta \theta$  for circular/arc type curves).

**Skill parameter of a sketch artist.** A single scalar  $\kappa \in \{1, \dots, 5\}$  modulates “hand skill”: lower  $\kappa \Rightarrow$  higher displacement amplitudes, more arc-length segments of a curve of length  $L$ , and more jitter. We use

$$\alpha(\kappa) = \frac{1}{5} (6 - \kappa) \in [0, 1],$$

and scale deviations by a base magnitude  $A_0(\kappa, L) = \alpha(\kappa) c_L L$  with  $c_L \in [10^{-3}, 10^{-2}]$  as a function parameter for different displacement fields according to skill.

**Straight line segments.** For line type curves, the displacement field  $\Delta \vec{u}_{\text{line}}$  contains a mean reverting random walk [59]  $\Delta \mathbf{u}_{\text{mr}}$ , end segment tapering  $\Delta \mathbf{u}_{\text{tpr}}$ , and a frequently bow-shaped bulge [19, 57]  $\Delta \mathbf{u}_{\text{bow}}$  fields along the  $u$ -direction and is capped within  $C \in [-c, c]$ . Next, a light tangential jitter  $\Delta \mathbf{t}_{\text{jitter}}$  is applied along the  $t$  direction. Finally, all displacement fields are smoothed using a moving average  $S_k$ , resulting in  $\Delta \vec{u}_{\text{line}}$ :

$$= \left[ \begin{array}{c} S_k(\text{clip}_c(\Delta \mathbf{u}_{\text{mr}}(s) + \Delta \mathbf{u}_{\text{bow}}(s)) + \Delta \mathbf{u}_{\text{tpr}}(s)) \\ \Delta \mathbf{t}_{\text{jitter}}(s) \end{array} \right] \quad (3)$$

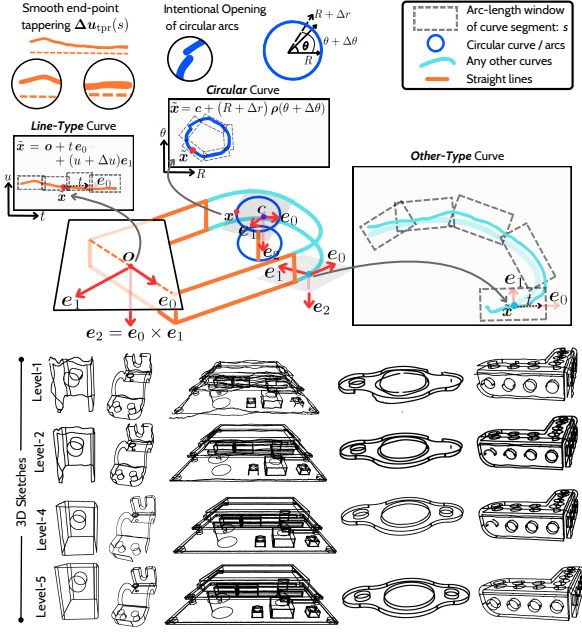


Figure 5. Five million sketches with BRep annotations

**Circular/arc segments.** For circle/arc type curves, we first fit the best circle  $(c, R, \theta)$  and re-parameterize it in polar form. Unlike line segments, several harmonics  $H_\theta$  are sampled to create bumps. Some arc-length segments are skipped to apply intentional openings. We set  $\Delta r = \Delta\theta_{\text{jit}} = 0$  at the start and end angles to avoid gaps. The radial and tangential jitters are linear projections onto tapered sinusoidal bases  $T(s)$  [20]. The points are lowered by  $\tilde{x} = c + (R + \Delta r)\rho(\theta + \Delta\theta_{\text{jit}})$ , with  $\rho$  the radial direction of the unit in the plane, resulting in  $\Delta\vec{u}_{\text{arc}}(s) = (\Delta r, \Delta\theta_{\text{jit}})^T$

$$= \begin{bmatrix} \mathbf{B}(\theta) & \mathbf{0} \\ \mathbf{0} & \mathbf{V}(\theta) \end{bmatrix} \begin{bmatrix} \mathbf{c}(s) \\ \mathbf{d}(s) \end{bmatrix} \text{ where,} \quad (4)$$

$$\mathbf{B} = \left[ \cos(\theta + \phi_1), \frac{1}{2} \sin(\theta + \phi_2), \right. \\ \left. \{\sin(k\theta + \psi_k), 0.6 \cos(k\theta + 0.73\psi_k)\}_{k=2}^{H_\theta} \right],$$

$\mathbf{c}(s) = [A\alpha_1, A\alpha_2, \{a_k T(s), a_k T(s)\}_{k=2}^{H_\theta}]$ ,  $\mathbf{V} = \{\sin(k\theta + \eta_k)\}_{k=1}^{H_\theta}$ , and  $\mathbf{d}(s) = \{\beta_k T(s)\}_{k=1}^{H_\theta}$ . This vector form preserves roundness while adding low-frequency wobble and tapered higher harmonics, as described in [20]. The curve bulging amplitudes  $\alpha_1, \alpha_2 \sim U[0.6, 1.0]$ . Similarly, the phase shifts  $\phi_1, \phi_2$  for lower harmonics and  $\eta_k, \psi_k$  for the higher harmonics adjust orientation of the sketching bulge.

**Other General curves.** For ellipses, B-Splines, or unknown curve types, we define a local arc-length segment and  $K$  number of small windows to apply multiple bows [19, 57], mean reversion, and tapering along the

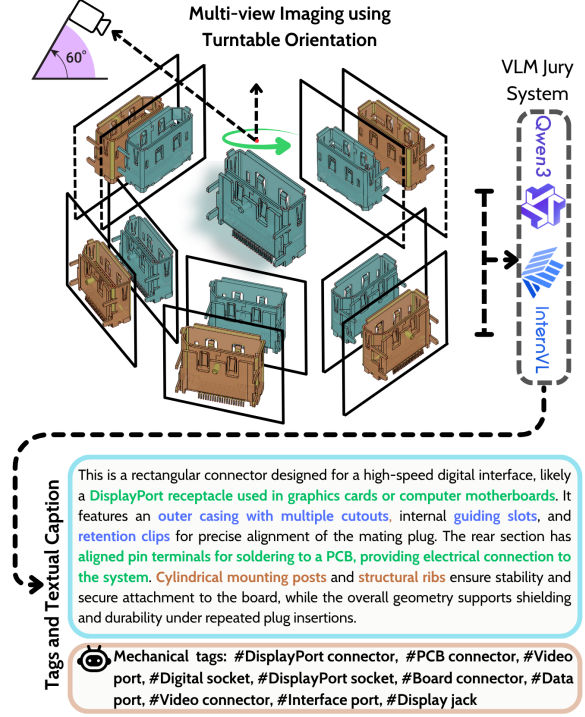


Figure 6. ~5K models of charging points, serial bus etc.

$u$ -direction, as defined in Eq. (3). The overlapping displacement fields are averaged to estimate  $\Delta\vec{u}_{\text{gen}}(s)$ .

### 3.4. Multi-view Images, Captions and Tags

High-fidelity 3D content generation from natural text prompts, *i.e.*, text-to-3D [26, 45, 55, 72], has rapidly advanced gaming, fashion, AR/VR, and filming industries [38]. However, apart from HoLA [44], no large-scale dataset provides visual elaborations of CAD models. Text2CAD [28], CAD-MLLM [68], and CADmium offer textual annotations only for *sequential design history* models in DeepCAD [67]. In A2Z, we employ a novel jury system of two state-of-the-art VLMs, Qwen3-14B [5, 71] and InternVL-26B [6], to generate high-quality captions and tags for all CAD models.

Our caption pipeline uses *twelve* multi-view images of each BRep, arranged in a 4x3 grid. As illustrated in Fig. 6, a turntable system captures transparently rendered BRep views with uniform and face-type color coding. This rendering comprehensively exposes inner primitives (e.g., loops, holes, shells, boundaries), enabling the VLM jury to (i) infer primitive details, (ii) identify real-world resemblance and use, (iii) highlight key surfaces, and (iv) describe the overall 3D structure.

The system also produces twenty concise tags per CAD model ( $\leq 3$  words each), serving as cross-references to industry terms. For example, tags like *bolt cutout*, *fitting cutout*, *prismatic cutout*, and *thread count*

or *cutout* allow efficient stocktaking and targeted asset management. Inspired by ImageNet [12] and WordNet [16], we organize tags into six feature classes – (i) Geometric Features, (ii) Miscellaneous, (iii) Mechanical Components, (iv) Structural Elements, (v) Electronic Components, and (vi) Fasteners – followed by four successive tree-structured category layers for systematic traversal and mining of the A2Z database (see supplement for analytics).

### 3.5. Annotating Electronic Enclosures

Three skilled designers created  $\sim 20\text{K}$  CAD models in Onshape [1] at  $\sim 900$  designs day, focusing on corner-rich parts of tablet and smartphone type casings. To design such models, an algorithmic variation of spline control points was created around the BRep faces at the corners, generating diverse geometries by preserving endpoint coincidence and  $G^1/G^2$  continuity constraints. Additionally,  $\sim 5\text{K}$  charging ports, sockets, and casings were also modeled to expand A2Z and strengthen CAD reverse engineering for high-demand categories. More results are also in the supplement.

## 4. Foundation Models for BRep Learning

**Boundary and Junction Detection.** We have implemented a baseline neural model with DGCNN [63] and two heads for detecting boundary and corner vertices, similar to ComplexGen [18], PieNet [62], and BRepDetNet [2], as a classical binary classification task. This is considered the most important step in training for other BRep primitive parsing and parametric fitting tasks [14, 15, 40, 53, 70]. We randomly selected 300K CAD models from the first and last thirty chunks of ABC and used our A2Z annotations to train the geometric deep learning model on two Nvidia H100 GPUs for just 20 epochs over four days. Our network architecture is similar to that of [2] and [62], with DGCNN [63] serving as the backbone module for point cloud encoding. Subsequently, the per-point binary classification task between boundary and non-boundary members, as well as the focal loss function, is also similar to those suggested in [2, 62] (for more details, see the supplement).

## 5. Benchmarking and Evaluation

We have carried out a thorough evaluation process to quantify the quality factor of our A2Z dataset and its annotations. Subsequently, we benchmark the performance of our foundation model against the baselines.

### 5.1. Quantitative Assessment on Dataset

**3D Scan and Sketch Annotation Assessment.** We assessed the visual quality of 3D scan annotations across BRep face IDs, face types, and 3D sketches of varying skill levels using three evaluators – (i) human feedback,

Method	Sketch Artist			
	Level	Gemini	GPT	Human
Face IDs	—	8.43	8.79	8.37
Face Type	—	7.88	8.71	8.05
	2	8.21	7.47	8.36
	3	7.87	7.71	9.12
Sketches	4	7.97	8.11	9.03
	5	8.31	8.43	9.61

Table 2. Visual quality scores (higher is better).

Level	MLTD	Unigram	Bigram	Method	ID	Type	Loop
Low	59.32	856	11355	Boundary	99.37	97.67	99.99
High	70.52	908	12181	Face	99.93	99.83	—

(a) Avg. MLTD [55] and uni/bigrams.

(b) Annotation coverage (%).

Table 3. Two tables highlights the lexical diversity (*left*) on captions and 3D scans’ annotation coverage statistics (*right*).

(ii) Gemini [58], and (iii) GPT-5 [50]. From 100 chunks of A2Z, we randomly sampled **10K** CAD models for this evaluation. A parallel visualization tool was developed to explore annotated 3D scans and original BRep files, and ten human participants rated the quality from 1 (poor) to 10 (best). Evaluation sessions were recorded for cross-reference, and the saved images were input into Gemini and GPT-5 for rating on the same scale. As shown in Tab. 2, GPT-5 scored face IDs and face types slightly higher than humans and Gemini. However, the overall consensus was consistent. For 3D sketches, Gemini and GPT scores rose only marginally between artist levels 2–5, while humans showed a clearer appreciation of artistic nuances (*More in the supplement*).

**Statistics on Annotation Coverage.** We quantify the completeness of 3D annotations as the percentage of accurate IDs of boundaries and faces present in our scan annotations (i.e., per vertex) compared to the ground truth CAD models (i.e., topological walk using ‘step’ files). This coverage is measured by averaging over the entire dataset. Tab. 3-(b) shows that we have almost perfect boundary coverage (ID: 99.37%, Type: 97.67%, Loop: 99.99%) as well as face coverage (ID: 99.93% and Type: 99.83%).

**Textual Caption Annotation Assessment.** Now, to assess the quality of our large corpus of textual annotations, we use the same 10K CAD samples and their captions (including tags). Next, Tab. 3-(a), we report n-gram statistics and lexical diversity (MLTD), following the protocol adopted in MARVEL-40M+[55]. To make a clear distinction between captions generated by a single small vision language model (SLM) Qwen-7B[71] and our jury system of two large VLMs, InternVL3-38B [6] and Qwen3-30B, we evaluate the metrics on both sets (see Tab. 3-(a)). We also observe that high-quality annotations (using InternVL3-38B[6] and Qwen3-30B[71]) yield a significantly better MLTD score (mean 70.52)

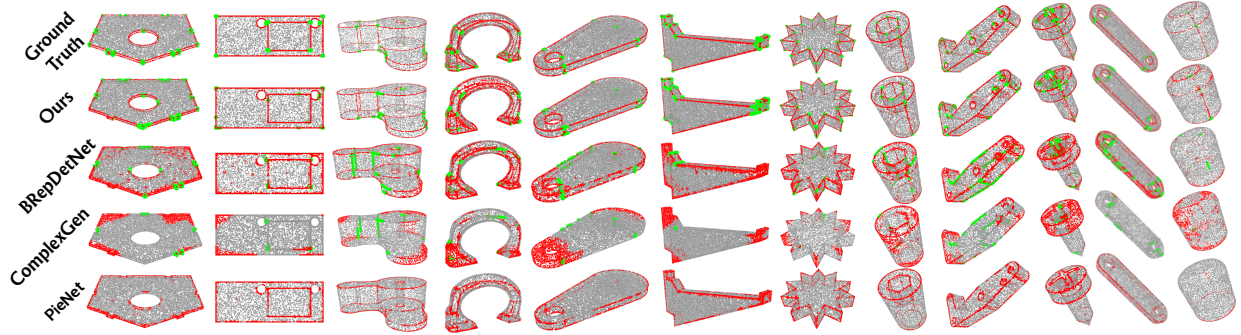


Figure 7. **Qualitative Comparison** of state-of-the-art methods in BRep *Boundary* and *Junction* classification as a downstream task.

Model	A2Z Chunks Seen (0–30, 70–99)				A2Z Chunks Unseen (31–69)			
	Boundary		Junction		Boundary		Junction	
	Recall	Precision	Recall	Precision	Recall	Precision	Recall	Precision
Ours	0.978	0.901	0.732	0.891	0.971	0.892	0.657	0.769
BRepDetNet*	0.903	0.781	0.454	0.561	0.873	0.701	0.353	0.426
BRepDetNet	0.593	0.511	0.355	0.231	0.571	0.529	0.311	0.226
ComplexGen*	0.551	0.750	0.297	0.592	0.521	0.646	0.212	0.465
ComplexGen	0.251	0.450	0.097	0.288	0.233	0.417	0.055	0.310
PieNet*	0.832	0.885	–	–	0.782	0.813	–	–
PieNet	0.738	0.840	–	–	0.699	0.806	–	–

Table 4. **Recall and Precision on A2Z:** Chunks Seen (0–30, 70–99) vs. Unseen (31–69). ■ = best, ■ = second best, ■ = N/A. The asterisk \* denotes freshly trained models on A2Z.

Model	CC3D Batches (0–10), 35K samples				Electronic Enclosure Chunk–100			
	Boundary		Junction		Boundary		Junction	
	Recall	Precision	Recall	Precision	Recall	Precision	Recall	Precision
Ours	0.961	0.854	0.633	0.810	0.934	0.898	0.725	0.873
BRepDetNet*	0.763	0.807	0.137	0.417	0.950	0.856	0.410	0.787
BRepDetNet	0.522	0.418	0.410	0.392	0.610	0.602	0.381	0.388
ComplexGen*	0.427	0.743	0.062	0.437	0.774	0.809	0.165	0.815
ComplexGen	0.280	0.444	0.011	0.388	0.221	0.491	0.028	0.320
PieNet*	0.663	0.843	–	–	0.680	0.870	–	–
PieNet	0.481	0.713	–	–	0.610	0.410	–	–

Table 5. Recall and Precision on **CC3D** [7] and **Electronic Enclosure** in the **zero-shot** setting.

compared to the low-quality condition (mean 59.33), resulting in a relative gain of 18.9%. While unigrams show a minor increase, there is a more significant increase in bigrams in high-quality annotations compared to low-quality ones. High-quality annotations clearly represent a more diverse corpus, as captured by the statistics.

## 5.2. Benchmarking Foundation Model

To assess the fidelity of BRep-to-scan supervision, we evaluated the performance of our proposed foundation model (Sec. 4) against PIE-Net [62], ComplexGen [18], and BRepDetNet [2] using their model check-points as well as a freshly trained model on our A2Z labels for boundary and corner detection tasks. CAD categories and types vary widely across 100 A2Z chunks, so performance is reported on the test sets ( $\sim 2K$  samples per chunk) over “seen” (0–30, 70–99) and “unseen” (31–69) chunks using recall–precision for boundary and junction vertices (see Tab. 4). Training utilized uniformly

sampled 10K scan points per shape and a batch size of 8 for the binary classification of boundary versus non-boundary. For the junction detection task, the process is conducted on top of the detected boundary points, following the same protocol. boundary vertices are sparse relative to all scan points, and junction vertices are even sparser relative to the boundaries, making corner detection particularly challenging for generic classifiers. Thanks to our high-quality annotations, the proposed model consistently achieves the highest recall–precision balance for both tasks on A2Z chunks (Tab. 4), on the CC3D dataset that was never used for training (Tab. 5), and on the newly added chunk for electronic enclosures.

When models from baseline methods are freshly trained, we see that [18] and [2] gain *recall-precision* in the ranges of  $\sim(10\%, 30\%)$  on the boundary task and  $\sim(4\%, 33\%)$  on the junction task. This is due to the remarkable quality of our annotations. The performance gain of PieNet [62] is no different from that of other methods on the boundary task. However, PieNet training and inference consistently fail in the junction task. Notably, the drop from seen to unseen chunks is smaller for our proposed approach than for the baselines. Qualitative results in Fig. 7 demonstrate cleaner boundary classification and more complete corner recovery by our model, with fewer spurious edges on planar faces and fewer missed junctions on A2Z test set. Collectively, the figure and table support the claim that the proposed foundation model can reliably transfer BRep topology cues to scans for downstream CAD reconstruction.

## 6. Conclusion and Future Work.

This work introduces a unique, most complete, and largest dataset of CAD and scan pairs with multimodal annotations. We conducted a thorough benchmarking of ground-truth annotations using Human feedback, GPT-5-based scoring, and the most suitable metrics to quantify the quality. Our foundation model and state-of-the-art results in boundary and junction classification demonstrate the value of this dataset for developing numerous new applications in generative BRep modeling, reverse engineering, and mining CAD features.

## 7. Acknowledgment

This project was primarily funded by BITS Pilani Hyderabad's NFSG Grant (Reference N4/24/1033). We are thankful to Vinci4D.ai for providing some CAD model samples of electronic enclosures.

## References

- [1] Onshape. <https://www.onshape.com/en/>. 2, 3, 7
- [2] Sk Aziz Ali, Mohammad Sadil Khan, and Didier Stricker. Brep boundary and junction detection for cad reverse engineering. In *2024 IEEE 3rd International Conference on Computing and Machine Intelligence (ICMI)*, pages 1–6, 2024. 2, 3, 7, 8
- [3] David Anderson, Yong Se Kim, and Sanjay Joshi. A discourse on geometric feature recognition from cad models. *Korea*, 440:746, 2001. 2
- [4] Autodesk. Autodesk Fusion 360 API . <https://autodeskfusion360.github.io/>, 2014. 3
- [5] Zhe Chen, Weiyun Wang, Hao Tian, Shenglong Ye, Zhangwei Gao, Erfei Cui, Wenwen Tong, Kongzhi Hu, Jiapeng Luo, Zheng Ma, et al. How far are we to gpt-4v? closing the gap to commercial multimodal models with open-source suites. *Science China Information Sciences*, 67(12):220101, 2024. 6, 14
- [6] Zhe Chen, Jiannan Wu, Wenhai Wang, Weijie Su, Guo Chen, Sen Xing, Muyan Zhong, Qinglong Zhang, Xizhou Zhu, Lewei Lu, et al. Internvl: Scaling up vision foundation models and aligning for generic visual-linguistic tasks. In *Proceedings of the IEEE/CVF conference on computer vision and pattern recognition*, pages 24185–24198, 2024. 6, 7
- [7] Kseniya Cherenkova, Djamila Aouada, and Gleb Gusev. Pvdeconv: Point-voxel deconvolution for autoencoding cad construction in 3d. pages 2741–2745, 2020. 3, 8, 20
- [8] Kseniya Cherenkova, Elona Dupont, Anis Kacem, Gleb A Gusev, and Djamila Aouada. Spelsnet: Surface primitive elements segmentation by b-rep graph structure supervision. In *The Thirty-eighth Annual Conference on Neural Information Processing Systems*, 2024. 2
- [9] John G Cherng, Xin-Yu Shao, Yubao Chen, and Peter R Sferro. Feature-based part modeling and process planning for rapid response manufacturing. *Computers & industrial engineering*, 34(2):515–530, 1998. 2, 15
- [10] Paul J. Curran. The semivariogram in remote sensing: An introduction. *Remote Sensing of Environment*, 24(3): 493–507, 1988. 5
- [11] Yongkang Dai, Xiaoshui Huang, Yunpeng Bai, Hao Guo, Hongping Gan, Ling Yang, and Yilei Shi. Brepformer: Transformer-based b-rep geometric feature recognition. In *Proceedings of the 2025 International Conference on Multimedia Retrieval*, page 155–163, New York, NY, USA, 2025. Association for Computing Machinery. 15
- [12] Jia Deng, Wei Dong, Richard Socher, Li-Jia Li, Kai Li, and Li Fei-Fei. Imagenet: A large-scale hierarchical image database. In *2009 IEEE Conference on Computer Vision and Pattern Recognition*, pages 248–255, 2009. 3, 7
- [13] Elona Dupont, Kseniya Cherenkova, Anis Kacem, Sk Aziz Ali, Ilya Aryhannikov, Gleb Gusev, and Djamila Aouada. Cadops-net: Jointly learning cad operation types and steps from boundary-representations. In *2022 International Conference on 3D Vision (3DV)*, 2022. 2
- [14] Eric-Tuan, Minhyuk Sung, Duygu Ceylan, Radomir Mech, Tamy Boubekeur, and Niloy J Mitra. Cpfm: Cascaded primitive fitting networks for high-resolution point clouds. In *Proceedings of the IEEE/CVF International Conference on Computer Vision*, pages 7457–7466, 2021. 2, 3, 7
- [15] Zheng Fang, Chuanqing Zhuang, Zhengda Lu, Yiqun Wang, Lupeng Liu, and Jun Xiao. Bgpseg: Boundary-guided primitive instance segmentation of point clouds. *IEEE Transactions on Image Processing*, 34:1454–1468, 2025. 2, 3, 7
- [16] C. Fellbaum. *WordNet: An Electronic Lexical Database*. Mit Press, 1998. 3, 7
- [17] T Flash and N Hogan. The coordination of arm movements: an experimentally confirmed mathematical model. *Journal of Neuroscience*, 5(7):1688–1703, 1985. 3
- [18] Haoxiang Guo, Shilin Liu, Hao Pan, Yang Liu, Xin Tong, and Baining Guo. Complexgen: Cad reconstruction by b-rep chain complex generation. *ACM Transactions on Graphics (TOG)*, 2022. 2, 3, 7, 8, 13
- [19] F.J. Harris. On the use of windows for harmonic analysis with the discrete fourier transform. *Proceedings of the IEEE*, 66(1):51–83, 1978. 3, 5, 6
- [20] Fredric J Harris. On the use of windows for harmonic analysis with the discrete fourier transform. *Proceedings of the IEEE*, 66(1):51–83, 2005. 6
- [21] Jingwei Huang, Yanfeng Zhang, and Mingwei Sun. Primitivenet: Primitive instance segmentation with local primitive embedding under adversarial metric. In *Proceedings of the IEEE/CVF International Conference on Computer Vision*, pages 15343–15353, 2021. 2, 3
- [22] Pradeep Kumar Jayaraman, Aditya Sanghi, Joseph G Lambourne, Karl DD Willis, Thomas Davies, Hooman Shayani, and Nigel Morris. Uv-net: Learning from boundary representations. In *Proceedings of the IEEE/CVF conference on computer vision and pattern recognition*, pages 11703–11712, 2021. 2, 3, 4
- [23] Pradeep Kumar Jayaraman, J. Lambourne, Nishkrit Desai, Karl D. D. Willis, Aditya Sanghi, and Nigel Morris. Solidgen: An autoregressive model for direct b-rep synthesis. *ArXiv*, abs/2203.13944, 2022. 3
- [24] Manuel Contero Jeffrey Otey, Pedro Company and Jorge D Camba. Revisiting the design intent concept in the context of mechanical cad education. *Computer-Aided Design and Applications*, 15(1):47–60, 2018. 2
- [25] Jing-En Jiang, Hanxiao Wang, Mingyang Zhao, Dong-Ming Yan, Shuangmin Chen, Shiqing Xin, Changhe Tu, and Wenping Wang. Defillet: Detection and removal of fillet regions in polygonal cad models. *ACM Transactions on Graphics (TOG)*, 44(4), 2025. 3

- [26] Rishabh Kabra, Loic Matthey, Alexander Lerchner, and Niloy J. Mitra. Leveraging vlm-based pipelines to annotate 3d objects. In *Proceedings of the 41st International Conference on Machine Learning*. PMLR, 2024. 6
- [27] Mohammad Sadil Khan, Elona Dupont, Sk Aziz Ali, Kseniya Cherenkova, Anis Kacem, and Djamila Aouada. Cad-signet: Cad language inference from point clouds using layer-wise sketch instance guided attention. In *Proceedings of the IEEE/CVF Conference on Computer Vision and Pattern Recognition (CVPR)*, 2024. 2
- [28] Mohammad Sadil Khan, Sankalp Sinha, Sheikh Talha Uddin, Didier Stricker, Sk Aziz Ali, and Muhammad Zeshan Afzal. Text2cad: Generating sequential CAD designs from beginner-to-expert level text prompts. In *Advances in Neural Information Processing Systems*, pages 7552–7579. Curran Associates, Inc., 2024. 3, 6
- [29] MA Kimmel, Mueed Ur Rehman, Yonatan Bisk, and Gary K. Fedder. Position: You can’t manufacture a nerf. In *Forty-second International Conference on Machine Learning Position Paper Track*, 2025. 2
- [30] Sebastian Koch, Albert Matveev, Zhongshi Jiang, Francis Williams, Alexey Artemov, Evgeny Burnaev, Marc Alexa, Denis Zorin, and Daniele Panozzo. Abc: A big cad model dataset for geometric deep learning. In *Proceedings of the IEEE/CVF conference on computer vision and pattern recognition*, pages 9601–9611, 2019. 2, 3
- [31] Joseph G Lambourne, Karl DD Willis, Pradeep Kumar Jayaraman, Aditya Sanghi, Peter Meltzer, and Hooman Shayani. Brepnet: A topological message passing system for solid models. In *Proceedings of the IEEE/CVF conference on computer vision and pattern recognition*, pages 12773–12782, 2021. 2
- [32] Joseph George Lambourne, Karl Willis, Pradeep Kumar Jayaraman, Longfei Zhang, Aditya Sanghi, and Kamal Rahimi Malekshan. Reconstructing editable prismatic cad from rounded voxel models. In *SIGGRAPH Asia 2022 Conference Papers*, pages 1–9, 2022. 3
- [33] Hyunoh Lee, Jinwon Lee, Hyunki Kim, and Duhwan Mun. Dataset and method for deep learning-based reconstruction of 3d cad models containing machining features for mechanical parts. *Journal of Computational Design and Engineering*, 9(1):114–127, 2021. 3
- [34] Jinwon Lee, Changmo Yeo, Sang-Uk Cheon, Jun Hwan Park, and Duhwan Mun. Brepnet: Graph neural network to segment machining feature faces in a b-rep model. *Journal of Computational Design and Engineering*, 10(6):2384–2400, 2023. 15
- [35] Mingi Lee, Dongsu Zhang, Clément Jambon, and Young Min Kim. Brepdiff: Single-stage b-rep diffusion model. In *Proceedings of the Special Interest Group on Computer Graphics and Interactive Techniques Conference Conference Papers*, New York, NY, USA, 2025. Association for Computing Machinery. 3
- [36] Changjian Li, Hao Pan, Adrien Bousseau, and Niloy J. Mitra. Sketch2cad: sequential cad modeling by sketching in context. *ACM Trans. Graph.*, 39(6), 2020. 3
- [37] Changjian Li, Hao Pan, Adrien Bousseau, and Niloy J. Mitra. Free2cad: Parsing freehand drawings into cad commands. *ACM Transactions on Graphics (TOG)*, 41(4):1–16, 2022. 3
- [38] Chenghao Li, Chaoning Zhang, Joseph Cho, Atish Waghvase, Lik-Hang Lee, Francois Rameau, Yang Yang, Sung-Ho Bae, and Choong Seon Hong. Generative ai meets 3d: A survey on text-to-3d in aigc era. *arXiv preprint arXiv:2305.06131*, 2023. 3, 6
- [39] Jing Li, Yihang Fu, and Falai Chen. DTGBrepGen: A Novel B-rep Generative Model through Decoupling Topology and Geometry. In *2025 IEEE/CVF Conference on Computer Vision and Pattern Recognition (CVPR)*, pages 21438–21447, Los Alamitos, CA, USA, 2025. IEEE Computer Society. 3
- [40] Lingxiao Li, Minhyuk Sung, Anastasia Dubrovina, L. Yi, and Leonidas J. Guibas. Supervised fitting of geometric primitives to 3d point clouds. *2019 IEEE/CVF Conference on Computer Vision and Pattern Recognition (CVPR)*, pages 2647–2655, 2018. 2, 3, 7
- [41] Pu Li, Wenhao Zhang, Jinglu Chen, and Dongming Yan. Stitch-a-shape: Bottom-up learning for b-rep generation. In *Proceedings of the Special Interest Group on Computer Graphics and Interactive Techniques Conference Conference Papers*, New York, NY, USA, 2025. Association for Computing Machinery. 3
- [42] Yuan Li, Cheng Lin, Yuan Liu, Xiaoxiao Long, Chenxu Zhang, Ningna Wang, Xin Li, Wenping Wang, and Xiaohu Guo. Caddreamer: Cad object generation from single-view images. In *Proceedings of the IEEE/CVF Conference on Computer Vision and Pattern Recognition (CVPR)*, pages 21448–21457, 2025. 3
- [43] Yujia Liu, Anton Obukhov, Jan Dirk Wegner, and Konrad Schindler. Point2cad: Reverse engineering cad models from 3d point clouds. In *Proceedings of the IEEE/CVF Conference on Computer Vision and Pattern Recognition (CVPR)*, pages 3763–3772, 2024. 2, 3, 13
- [44] Yilin Liu, Duoteng Xu, Xingyao Yu, Xiang Xu, Daniel Cohen-Or, Hao Zhang, and Hui Huang. Hola: B-rep generation using a holistic latent representation. *ACM Trans. Graph.*, 44(4), 2025. 3, 6
- [45] Tiange Luo, Chris Rockwell, Honglak Lee, and Justin Johnson. Scalable 3d captioning with pretrained models. In *Proceedings of the 37th International Conference on Neural Information Processing Systems*, Red Hook, NY, USA, 2023. Curran Associates Inc. 6
- [46] Weijian Ma, Minyang Xu, Xueyang Li, and Xiangdong Zhou. Multicad: Contrastive representation learning for multi-modal 3d computer-aided design models. In *Proceedings of the 32nd ACM International Conference on Information and Knowledge Management*, page 1766–1776, New York, NY, USA, 2023. Association for Computing Machinery. 2
- [47] Dimitrios Mallis, Ali Sk Aziz, Elona Dupont, Kseniya Cherenkova, Ahmet Serdar Karadeniz, Mohammad Sadil Khan, Anis Kacem, Gleb Gusev, and Djamila Aouada. Sharp challenge 2023: Solving cad history and parameters recovery from point clouds and 3d scans. overview, datasets, metrics, and baselines. In *Proceedings of the IEEE/CVF International Conference on Computer Vision*, pages 1786–1795, 2023. 2, 3

- [48] Albert Matveev, Ruslan Rakhimov, Alexey Artemov, Gleb Bobrovskikh, Vage Egiazarian, Emil Bogomolov, Daniele Panozzo, Denis Zorin, and Evgeny Burnaev. Def: Deep estimation of sharp geometric features in 3d shapes. *ACM Transactions on Graphics (TOG)*, 2022. 3
- [49] J. J. Monaghan. Smoothed particle hydrodynamics. *Annual Review of Astronomy and Astrophysics*, 30(Volume 30, 1992):543–574, 1992. 4
- [50] Josh OpenAI, Achiam, Steven Adler, Sandhini Agarwal, Lama Ahmad, Ilge Akkaya, Florencia Leoni Aleman, Diogo Almeida, Janko Altschmidt, Sam Altman, Shyamal Anadkat, et al. Gpt-4 technical report. *arXiv preprint arXiv:2303.08774*, 2023. 3, 7, 17
- [51] Ken Perlin. An image synthesizer. In *Proceedings of the 12th Annual Conference on Computer Graphics and Interactive Techniques*, page 287–296, New York, NY, USA, 1985. Association for Computing Machinery. 4
- [52] Bonsa Regassa Hunde and Abraham Debebe Woldeyohannes. Future prospects of computer-aided design (cad) – a review from the perspective of artificial intelligence (ai), extended reality, and 3d printing. *Results in Engineering*, 14:100478, 2022. 2, 15
- [53] Gopal Sharma, Difan Liu, Subhransu Maji, Evangelos Kalogerakis, Siddhartha Chaudhuri, and Radomír Měch. Parsenet: A parametric surface fitting network for 3d point clouds. In *Computer Vision–ECCV 2020: 16th European Conference, Glasgow, UK, August 23–28, 2020, Proceedings, Part VII 16*. Springer, 2020. 2, 7
- [54] Jonathon Shlens. A tutorial on principal component analysis. *ArXiv*, abs/1404.1100, 2014. 5
- [55] Sankalp Sinha, Mohammad Sadil Khan, Muhammad Usama, Shino Sam, Didier Stricker, Sk Aziz Ali, and Muhammad Zeshan Afzal. Marvel-40m+: Multi-level visual elaboration for high-fidelity text-to-3d content creation. In *Proceedings of the IEEE/CVF Conference on Computer Vision and Pattern Recognition (CVPR)*, pages 8105–8116, 2025. 6, 7
- [56] Binil Starly, Akshay G. Bharadwaj, and Atin Angrish. Fabwave cad repository categorized part classes - cad 1 through 15 classes (part 1/3). 2019. 3
- [57] R. Sturgis and F.A. Davis. *Sturgis’ Illustrated Dictionary of Architecture and Building: An Unabridged Reprint of the 1901-2 Edition*. Dover Publications, 2013. 5, 6
- [58] Gemini Team. Gemini: A family of highly capable multimodal models, 2024. 3, 7
- [59] G. E. Uhlenbeck and L. S. Ornstein. On the theory of the brownian motion. *Phys. Rev.*, 36:823–841, 1930. 5
- [60] Mikaela Angelina Uy, Yen-Yu Chang, Minhyuk Sung, Purvi Goel, Joseph G Lambourne, Tolga Birdal, and Leonidas J Guibas. Point2cyl: Reverse engineering 3d objects from point clouds to extrusion cylinders. In *Proceedings of the IEEE/CVF Conference on Computer Vision and Pattern Recognition*, pages 11850–11860, 2022. 2
- [61] Cheng Wang, Xinzhu Ma, Bin Wang, Shixiang Tang, Yuan Meng, and Ping Jiang. Point2Primitive: CAD Reconstruction from Point Cloud by Direct Primitive Prediction. *arXiv e-prints*, art. arXiv:2505.02043, 2025. 2, 13
- [62] Xiaogang Wang, Yuelang Xu, Kai Xu, Andrea Tagliasacchi, Bin Zhou, Ali Mahdavi-Amiri, and Hao Zhang. Pienet: Parametric inference of point cloud edges. *Advances in neural information processing systems*, 33: 20167–20178, 2020. 3, 7, 8
- [63] Yue Wang, Yongbin Sun, Ziwei Liu, Sanjay E. Sarma, Michael M. Bronstein, and Justin M. Solomon. Dynamic graph cnn for learning on point clouds. *ACM Transactions on Graphics (TOG)*, 2019. 7
- [64] Kevin J Weiler. *Topological structures for geometric modeling (Boundary representation, manifold, radial edge structure)*. Rensselaer Polytechnic Institute, 1986. 2
- [65] Karl DD Willis, Yewen Pu, Jieliang Luo, Hang Chu, Tao Du, Joseph G Lambourne, Armando Solar-Lezama, and Wojciech Matusik. Fusion 360 gallery: A dataset and environment for programmatic cad construction from human design sequences. *ACM Transactions on Graphics (TOG)*, 40(4):1–24, 2021. 2, 3
- [66] Jo Wood, Petra Isenberg, Tobias Isenberg, Jason Dykes, Nadia Boukhelifa, and Aidan Slingsby. Sketchy rendering for information visualization. *IEEE Transactions on Visualization and Computer Graphics*, 18(12):2749–2758, 2012. 3
- [67] Rundi Wu, Chang Xiao, and Changxi Zheng. Deepcad: A deep generative network for computer-aided design models. In *Proceedings of the IEEE/CVF International Conference on Computer Vision (ICCV)*, pages 6772–6782, 2021. 2, 6
- [68] Jingwei Xu, Chenyu Wang, Zibo Zhao, Wen Liu, Yi Ma, and Shenghua Gao. Cad-mlm: Unifying multimodality-conditioned cad generation with mlm. *arXiv preprint arXiv:2411.04954*, 2024. 6
- [69] Xiang Xu, Joseph Lambourne, Pradeep Jayaraman, Zhengqing Wang, Karl Willis, and Yasutaka Furukawa. Brepgen: A b-rep generative diffusion model with structured latent geometry. *ACM Transactions on Graphics (TOG)*, 43(4):1–14, 2024. 3
- [70] Siming Yan, Zhenpei Yang, Chongyang Ma, Haibin Huang, Etienne Vouga, and Qi-Xing Huang. Hpnet: Deep primitive segmentation using hybrid representations. 2021 ieee. In *CVF International Conference on Computer Vision (ICCV)(2021)*, pages 2733–2742, 2021. 2, 7
- [71] An Yang, Anfeng Li, Baosong Yang, Beichen Zhang, Binyuan Hui, Bo Zheng, Bowen Yu, Chang Gao, Chengen Huang, Chenxu Lv, et al. Qwen3 technical report. *arXiv preprint arXiv:2505.09388*, 2025. 6, 7, 14, 15, 16
- [72] Longwen Zhang, Ziyu Wang, Qixuan Zhang, Qiwei Qiu, Anqi Pang, Haoran Jiang, Wei Yang, Lan Xu, and Jingyi Yu. Clay: A controllable large-scale generative model for creating high-quality 3d assets. *ACM Trans. Graph.*, 43(4), 2024. 6
- [73] Shengdi Zhou, Tianyi Tang, and Bin Zhou. Cadparser: A learning approach of sequence modeling for b-rep cad. 2, 3

# A2Z-10M+: Geometric Deep Learning with A-to-Z BRep Annotations for AI-Assisted CAD Modeling and Reverse Engineering

## Supplementary Material

### Contents

<b>A Multi-scale SPH for Neighbor Labeling</b>	<b>12</b>
A.1 Coedge Length–Aware Neighbors. . . . .	12
A.2 SPH kernel with BRep Surface features. .	12
<b>B Synthesized Sketch and Realism Analysis</b>	<b>13</b>
B.1. Generation Pipeline . . . . .	13
B.2. Quantitative Realism Evaluation . . . . .	13
<b>C Synthesized Scan and Realism Analysis</b>	<b>13</b>
C.1. Artec3D-Calibrated Scan Synthesis . . .	13
C.2. Stage-Wise Realism Evaluation . . . . .	14
<b>D Prompt for CAD Description and Tags</b>	<b>14</b>
D.1. Description . . . . .	15
D.2 Applying Filtering and Constraints . . .	15
D.3 Output Format . . . . .	15
<b>E Hierarchical Tags for CAD Retrieval</b>	<b>15</b>
E.1. Semantic Hierarchy over 1M A2Z Models	16
E.2. Heterogeneous Graph Representation . .	17
E.3. Graph Mining and Retrieval Mechanism .	17
<b>F. GPT-5, Gemini, and Human Evaluation.</b>	<b>17</b>
F.1. Chunk-wise Evaluation of Model . . . . .	17
<b>G More Examples of Caption and Tags</b>	<b>18</b>
<b>H More Examples of Electronic Enclosures</b>	<b>18</b>
<b>I. Examples of Annotations and Predictions</b>	<b>18</b>

We structure the supplementary material according to the content outlined above.

#### A. Multi-scale SPH for Neighbor Labeling

In A2Z, we have generated 3D meshes that closely resemble real-world scanning outcomes. This process is carried out by uniquely combining multiple computational geometry algorithms, guided by BRep geometry and topology features. Many uncommon problems arise when too many small faces are adjacent to one another. These corner cases create confusion about how to assign the nearest neighbor. Let  $\mathcal{P} = \{\mathbf{p}_i\}_{i=1}^N$  be the scan, and let  $\mathbf{x} \in \mathcal{S}_E \cup \mathcal{S}_F$  be a sampled BRep point with local frame  $R(\mathbf{x}) = [\mathbf{t}, \mathbf{u}, \mathbf{n}]$  (tangent, in-plane, normal).

#### A.1. Coedge Length{Aware Neighbors.

For a boundary sample  $\mathbf{x} \in \mathcal{S}_E$  with parent edge length  $L_{e(\mathbf{x})}$ , we first define a base scale  $h_E(\mathbf{x}) = \alpha_E L_{e(\mathbf{x})}$ ,  $\mathcal{R}_E(\mathbf{x}) = \{r_k(\mathbf{x}) = \gamma_k h_E(\mathbf{x})\}_{k=1}^K$ , and then for a BRep face sample point  $\mathbf{x} \in \mathcal{S}_F$  with grid pitch  $\Delta_f$ , the same base scale for the face is defined as:

$$h_F(\mathbf{x}) = \alpha_F \Delta_f \text{ and } \mathcal{R}_F(\mathbf{x}) = \{r_k(\mathbf{x}) = \gamma_k h_F(\mathbf{x})\}_{k=1}^K.$$

Next, an anisotropic metric along the BRep edge measures whether small gaps exist of the two adjacent faces are kind of "seam edges",

$$d_i(\mathbf{x}) = \|\mathbf{p}_i - \mathbf{x}\|_{A(\mathbf{x})} = \sqrt{(\mathbf{p}_i - \mathbf{x})^\top A(\mathbf{x})(\mathbf{p}_i - \mathbf{x})},$$

$$A(\mathbf{x}) = R(\mathbf{x}) \text{diag}(\sigma_t^{-2}, \sigma_u^{-2}, \sigma_n^{-2}) R(\mathbf{x})^\top.$$

with  $\sigma_t > \sigma_u \geq \sigma_n$  on the edges and  $A(\mathbf{x}) \propto I$  on the BRep faces. Once

#### A.2. SPH kernel with BRep Surface features.

We use the cubic-spline SPH kernel in 3D,

$$W(q, h) = \frac{1}{\pi h^3} \begin{cases} 1 - \frac{3}{2}q^2 + \frac{3}{4}q^3, & 0 \leq q < 1, \\ \frac{1}{4}(2 - q)^3, & 1 \leq q < 2, \\ 0, & q \geq 2, \end{cases}$$

with  $q = d_i(\mathbf{x})/h$ . Non-sharp operational features (filets, chamfers, bosses) receive a curvature-aware smoothing length

$$h(\mathbf{x}) = \eta \min(h_*(\mathbf{x}), R_\kappa(\mathbf{x})),$$

$$R_\kappa(\mathbf{x}) = \frac{1}{\max(|\kappa_1(\mathbf{x})|, |\kappa_2(\mathbf{x})|, \varepsilon)}.$$

where  $h_* \in \{h_E, h_F\}$  and  $\kappa_{1,2}$  are the principal curvatures from the B-Rep surface at  $\mathbf{x}$ .

Optionally, a normal-consistency gate improves robustness near joints:

$$g_i(\mathbf{x}) = \exp(-\lambda [1 - |\mathbf{n}(\mathbf{x})^\top \mathbf{n}_i|]),$$

where  $\mathbf{n}_i$  is the scan normal at  $\mathbf{p}_i$  (if available). The anisotropic metric  $A(\mathbf{x})$  and the SPH kernel  $W(q, h)$  jointly ensure coverage of close-proximity vertices and accurate recovery on smooth CAD features without overextending across sharp boundaries, as described in **Eq. 2** of the main matter.

## B. Synthesized Sketch and Realism Analysis

A critical modality in A2Z-10M+ is the *sketch*, which bridges the gap between early-stage conceptual design and precise BRep geometry. Sketches in engineering practice span a wide stylistic spectrum—from quick freehand concept doodles to dimensioned orthographic projections—and a dataset that targets sketch-based CAD retrieval and reconstruction must faithfully cover this range.

### B.1. Generation Pipeline

A2Z adopts a multi-level 3D sketching framework (Sec. 3.3 of the main paper) that builds on recent advances in differentiable stroke rendering. Beginning from the native BRep representation, the pipeline proceeds through four stages:

1. **View capture.** A set of canonical viewpoints is sampled around the CAD model, and perspective/orthographic projections are rendered, preserving the association between projected curves and their parent BRep edges.
2. **Occlusion removal.** Hidden lines are identified via depth-buffer queries and either removed (for engineering-style drawings) or rendered with dashed strokes (for see-through conceptual sketches).
3. **Loop pruning.** Redundant or visually cluttered silhouette loops are simplified while retaining topologically significant contours (e.g., holes, fillets, chamfer boundaries).
4. **Stroke rendering.** The surviving curves are rasterized with stylistic variation (line weight jitter, over-sketching, slight positional noise) to approximate hand-drawn appearance at multiple fidelity levels.

The result is a hierarchy of sketch abstractions—referred to as *Level-2* through *Level-5* in decreasing order of realism—each retaining the semantic edge-type and edge-ID labels inherited from the parent BRep. This label preservation is essential: while pixelated sketches are sufficient for image-based *retrieval*, they cannot drive BRep *reconstruction* without the accompanying semantic edge annotations that specify curve type (line, arc, B-spline), connectivity, and face adjacency.

### B.2. Quantitative Realism Evaluation

To validate sketch realism, we conducted a perceptual evaluation on a held-out set of 5 000 newly generated 2D sketches (half of our evaluation pool, corresponding to ll. 455–464 of the main paper). Each sketch was scored on a 1–10 realism scale by three independent evaluators: two frontier vision-language models (GPT-5, Gemini) acting as automated raters, and a panel of mechanical engineering graduate students serving as human raters.

Table 6 reports the mean and standard deviation per abstraction level.

Several trends emerge. First, *Level-2* sketches, which retain the most geometric detail, receive high scores from automated raters but are judged slightly lower by humans, likely because the density of strokes can appear mechanical rather than hand-drawn. Second, *Level-3* achieves the strongest overall evaluator consensus: it retains enough salient contours for reliable part identification while introducing sufficient stylistic abstraction to appear natural. Third, at the more abstracted *Level-4* and *Level-5*, human raters remain relatively tolerant (scores above 7.6), whereas automated raters penalize the loss of geometric detail more sharply; this gap highlights a known limitation of VLM-based perceptual metrics, which tend to favour high-frequency detail.

These results confirm that the multi-level sketching pipeline produces perceptually convincing outputs across the realism spectrum, supporting both downstream retrieval tasks (where coarse sketches suffice) and reconstruction tasks (where *Level-2/3* sketches with full semantic labels are preferred).

## C. Synthesized Scan and Realism Analysis

The second critical modality in A2Z-10M+ is the *synthesized 3D scan*, which simulates the output of real structured-light or laser-based acquisition devices applied to CAD parts. High-fidelity synthetic scans are essential for training and evaluating scan-to-BRep reconstruction methods [18, 43, 61], yet prior datasets typically add only simple Gaussian noise to uniformly sampled point clouds—a poor proxy for the spatially correlated artefacts produced by physical sensors.

### C.1. Artec3D-Calibrated Scan Synthesis

A2Z addresses this gap through a four-stage scan synthesis algorithm (Sec. 3.1 of the main paper) whose parameters are calibrated against ground-truth (GT) scans produced by the Artec3D virtual scanner. Artec3D is a proprietary tool that replicates the optical path, sensor calibration curves, and opto-photonics noise characteristics of its commercial structured-light hardware; scans produced by this tool are therefore treated as *real ground truth* for evaluation purposes. The four stages introduce progressively more realistic artefacts:

1. **Step I (Uniform sampling & base noise).** Points are sampled uniformly on the BRep surface and perturbed with isotropic Gaussian noise calibrated to the Artec3D sensor’s baseline repeatability specification.
2. **Step II (View-dependent density).** A virtual sensor viewpoint is introduced, and point density is modulated by the local surface-to-sensor angle, replicating the reduced sampling density observed on oblique

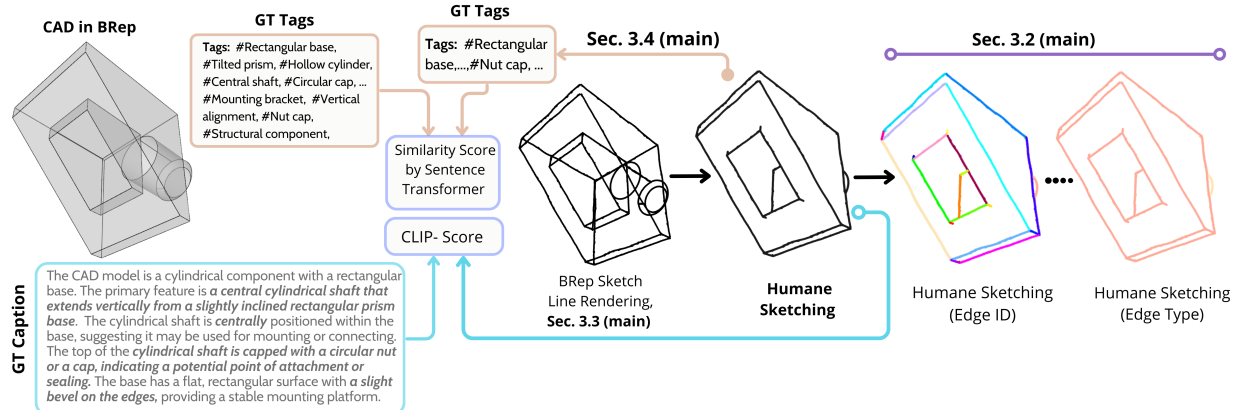


Figure 8. **Realism of Sketch.**: We compute a CLIP cosine-similarity score of **30.58** between generated captions and the corresponding 2D sketches, confirming that textual descriptions are well-grounded in visual content. Additionally, a tag-level similarity score of **64.7%** (CAD-derived tags vs. sketch-derived tags) demonstrates that the hierarchical tag vocabulary remains consistent across the BRep and sketch modalities.

Evaluator	Modality	Level-2	Level-3	Level-4	Level-5
GPT-5	sketch	7.65 ± 0.34	7.20 ± 0.48	5.53 ± 0.38	5.05 ± 0.39
Gemini	sketch	<b>9.01 ± 0.28</b>	7.33 ± 0.52	6.06 ± 0.58	3.92 ± 0.47
Human	sketch	7.20 ± 0.32	<b>7.86 ± 0.38</b>	7.85 ± 0.44	7.67 ± 0.71

Table 6. Realism scores (mean ± std, 1–10 scale) for *multi-level 2D sketches* evaluated by automated VLM raters and human engineering students. Higher is better. Level-3 achieves the strongest evaluator consensus, balancing abstraction with recognizability.

and self-occluded regions.

- Step III (Structured artefacts).** Spatially correlated noise patterns—edge ringing, specular dropout, and inter-reflection ghosts—are layered according to material BRDF models and local curvature, emulating systematic scanner errors absent from i.i.d. noise models.
- Step IV (Full sensor simulation).** The complete Artec3D opto-photonic pipeline is applied, including lens distortion, structured-light fringe decoding residuals, and outlier generation at depth discontinuities, yielding scans that closely match real GT.

## C.2. Stage-Wise Realism Evaluation

To quantify the realism gain at each stage, we synthesized scans from CC3D CAD models whose Artec3D GT scans are available. We evaluated each stage using the same three-evaluator protocol described in Sec. B.2, *i.e.*, automated VLM raters and human experts. The Table 7 reports the results employing the visual comparison tool shown in Fig. 10.

The results reveal a clear monotonic improvement in perceived realism across stages. Steps I and II, which model only point distribution and view-dependent density, receive modest scores (6.3–7.9), indicating that

density variation alone is insufficient to fool either human or automated raters. The introduction of structured artefacts in Step III yields a noticeable jump (roughly +1 point across all evaluators), confirming that spatially correlated sensor errors are a primary perceptual cue for scan authenticity. Finally, Step IV achieves near-ceiling scores— $9.83 \pm 0.22$  from human raters—demonstrating that the full opto-photonic simulation produces scans virtually indistinguishable from real Artec3D acquisitions.

The extremely low variance at Step IV for human raters ( $\sigma = 0.22$ ) is particularly noteworthy: it indicates strong inter-annotator agreement that the synthesized scans are realistic, providing a high-confidence quality floor for downstream learning tasks such as boundary detection, surface segmentation, and BRep fitting.

## D. Prompt for CAD Description and Tags

We have structured our prompt template for a mixture of VLMs – Qwen3-30B [71] and InternVL3 [5] (see Section 3.4 of the main matter)—and defined a consistent textual description and tag set. In the prompt template, the following segments are present:

Evaluator	Modality	Step-I	Step-II	Step-III	Step-IV
GPT-5	scan	6.51 ± 0.84	6.54 ± 1.01	7.58 ± 0.58	<b>9.41 ± 0.60</b>
Gemini	scan	7.73 ± 1.48	7.91 ± 0.92	8.54 ± 0.78	<b>9.28 ± 0.81</b>
Human	scan	6.32 ± 0.29	6.58 ± 0.80	7.20 ± 0.51	<b>9.83 ± 0.22</b>

Table 7. Realism scores (mean ± std, 1–10 scale) for *synthesized scans* at each pipeline stage, evaluated against Artec3D ground-truth scans of CC3D models. Refer to Figure. 12 for visuals. **Step IV** achieves near-perfect human consensus.

#### Overall LLM’s Role

“You are a senior mechanical design engineer with deep expertise in component identification and sourcing. You are shown 12 images of a single CAD model from multiple views, arranged in a grid. Your task is to analyse the geometry and produce a technical description and classification tags suitable for a professional engineering database”.

After defining the role, we fix the rules for the description in in-context prompt learning in three different parts: (1) Description, (2) Filtering and Constraints, and (3) Desired Output Structure.

### D.1. Description

Write a single, concise paragraph (maximum 150 words) that follows these guidelines:

- Primary identification.** Use specific, standard mechanical terminology only when the geometry makes the class obvious; if the type is unclear, describe the geometry directly and do *not* speculate about its industry role.
- Justification and geometry.** Justify your identification by describing the key geometric features that support it. If you cannot confidently name the part, instead of describing its dominant geometric forms (cylinders, prisms, ...) and their spatial relationships using CAD terms (concentric, axial, radial, ...).
- Feature details.** Mention mounting features, holes, cut-outs, bosses, slots, or surface transitions (files, chamfers, ...) that appear critical to the part’s function.
- Synthesis of views.** Ensure that the description is a cohesive synthesis of all views, explicitly noting overall symmetries and important spatial relationships.
- Potential application:** Briefly state a plausible industrial application or use case, and the likely engineering function of the component based on its geometry.

### D.2. Applying Filtering and Constraints

#### Filtering and Constraints

We have implemented some restrictions and ethical filtering constraints for Qwen3-30B [71] to generate the final response. For instance,

- Do **not** use canned template phrases such as “This appears to be a ... shaft coupling” or “The component is a ... cylinder” unless the object is genuinely that specific type. Be original in your wording.
- The final tag list must contain 20 items in a flat structure. Do not include headings like “Category/Class:” in the output.
- Avoid generic, overused terms (e.g., *flange*, *bracket*, *housing*) unless the geometry explicitly and unambiguously matches those features, and you are more than 90% confident.

### D.3. Output Format

The response must follow this exact structure:

#### Output Structure

```
Description: {Your paragraph here}
Tags:
- Tag 1
- Tag 2
- ...
- Tag 10
```

### E. Hierarchical Tags for CAD Retrieval

Geometric feature recognition [11, 52] on BRep, and then streamlining those features to replace traditional part modeling techniques [9], can transform complex CAD retrieval for reuse purposes in design. Like many other important downstream tasks of BRep learning the retrieval and identification of CAD models by their geometric features [34] automate manufacturing steps by saving time and reducing human error. For this purpose, a well-structured database of part components is necessary for ingestion. Such a database serves as a go-to reference that links the Computer-Aided Design (CAD)

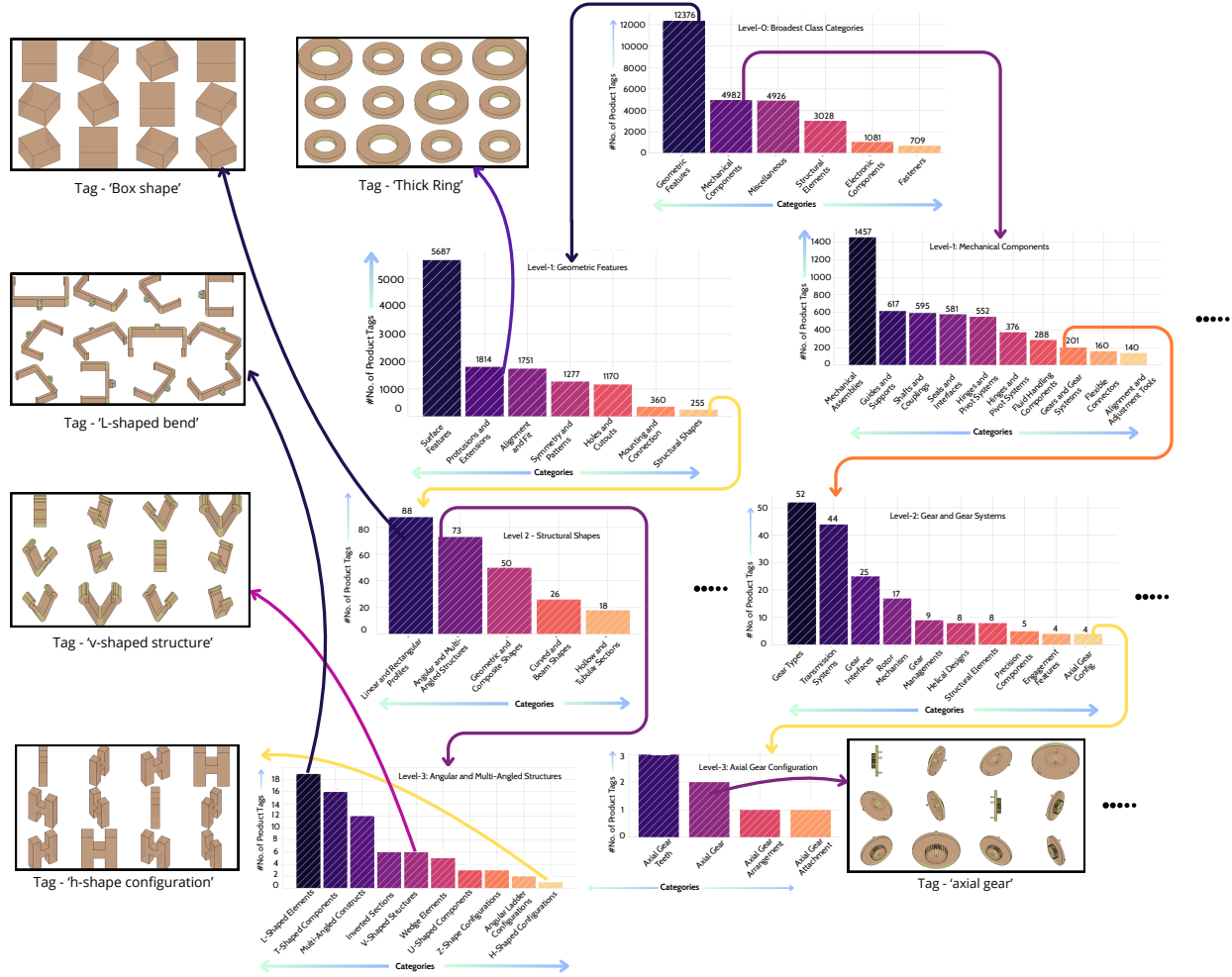


Figure 9. Hierarchical categorization of 1 million CAD models for retrieval and causal mining. The two examples illustrate how – (*on the right*) one can fetch some CAD models when asked to find – ‘A *mechanical component* associated to *Gear type transmission* systems supporting *Axial* rotation’.

process to the Computer-Aided Manufacturing (CAM) workflow. Our methodology for this hierarchical mining and retrieval of CAD based on their captions and unique tags is described below:

### E.1. Semantic Hierarchy over 1M A2Z Models

We begin with a corpus of roughly one million CAD models from the ABC dataset, each annotated with a visual caption and up to ten free-form tags, as mentioned in the main matter. An initial test run is first made on the  $N = 27,102$  distinct tags that appear throughout the corpus. We construct a semantic hierarchy that simultaneously reflects human design intuition and the empirical distribution of the data. We iteratively use Qwen3–30B [71] as an LLM to serve as a semantic classifier, running over  $\lfloor \frac{N}{100} \rfloor$  unique tags in a chunk and then clustering them consistently across other chunks. Therefore, we have created semantic clustering with a maximum depth of 5 in distinct phases.

**Phase-1: high-level assignment.** Every tag  $t$  is first routed into one of  $K$  coarse parent categories  $\{c_1, \dots, c_K\}$  (e.g., *Geometric Features*, *Mechanical Components*, *Structural Elements*, *Electronic Components*, *Fasteners*, plus an *Unclassified* bucket). The model is prompted with the tag in isolation and returns a single category label, yielding a mapping

$$\phi_1 : t \mapsto c_k.$$

This step ensures that all later reasoning is constrained within a semantically coherent region of the space.

**Phase-2: recursive refinement.** Within each coarse category, we recursively subdivide tag sets into more specific groups. Given a set  $S \subset \mathcal{T}$  of tags that share the same parent, the LLM is asked to propose between five and ten meaningful sub-groups that partition  $S$  (e.g., under *Geometric Features*, we obtain groups such as *box-like shapes*, *L-bends*, *V-shaped structures*, and *axial gears*, as shown in Fig. 9). The process is repeated for

Table 8. Distribution of the 27,102 unique tags over top-level categories and their Percentage (%) of CAD models.

Category	Tag Count	Percentage
Geometric Features	12,230	45.13%
Unclassified	6,068	22.39%
Mechanical Components	4,601	16.98%
Structural Elements	2,724	10.05%
Electronic Components	801	2.96%
Fasteners	678	2.50%

each child group until either (i) the group contains fewer than ten tags or (ii) a maximum depth is reached. The result is an irregular, data-driven tree that is deep where the vocabulary is rich and shallow where it is sparse.

**Phase-3: attaching model identifiers.** After the structure of the tree is fixed, we traverse it and for each leaf node  $\nu$  we attach the set of CAD models

$$\mathcal{M}_\nu = \{m \in \mathcal{M} \mid \text{tag}(m) \ni t \text{ and } t \in \nu\}$$

that carry any of the tags stored at  $\nu$ . As a consequence, every model is reachable from multiple semantic leaves, coupling fine-grained vocabulary (e.g., “axial gear with keyway”) with the raw geometry of the associated CAD.

**Phase 4: statistical reporting.** Finally, the fully assembled hierarchy is summarized to support downstream analysis and dataset curation. Table 8 reports the observed distribution of tags over the root categories, revealing, for instance, that nearly half of all tags are geometric in nature, while mechanical and structural terms jointly account for roughly one quarter of the vocabulary. These statistics are later used to rebalance training sets and design retrieval strategies that avoid overfitting to overrepresented classes.

## E.2. Heterogeneous Graph Representation

The hierarchical taxonomy is converted into a heterogeneous graph that unifies tags, categories, captions, and CAD models. Let  $\mathcal{M}$  denote the set of model nodes,  $\mathcal{T}$  the set of tag nodes, and  $\mathcal{C}$  the set of category nodes (internal and root). The vertex set is

$$V = \mathcal{M} \cup \mathcal{T} \cup \mathcal{C},$$

and the edge set  $E$  contains four main relation types:

1. **Taxonomic edges** ( $c_{\text{parent}}, c_{\text{child}}$ ) encode the “is-a” relation of the hierarchy tree.
2. **Tag–category edges** ( $t, c$ ) for every tag  $t$  assigned to a leaf category  $c$ .
3. **Model–tag edges** ( $m, t$ ) whenever the model  $m$  carries the tag  $t$ .
4. **Co-occurrence edges** ( $t_i, t_j$ ) with weight  $w_{ij}$  proportional to the point-wise mutual information or normalized co-frequency of  $t_i$  and  $t_j$  across models.

In the future, we aim to equip each node with learned feature vectors, *i.e.*, text embeddings generated using their captions passed through a foundational model like GPT[50]. The resulting structure is a richly typed knowledge graph that captures both symbolic semantics (“V-shaped structural bracket”) and descriptions.

## E.3. Graph Mining and Retrieval Mechanism

Given this representation, both discovery and retrieval reduce to structured navigation over the graph. **Mining semantic and geometric patterns.** We apply community detection and frequent subgraph mining to the tag-tag and model-tag subgraphs to uncover recurrent design motifs. For example, high-weight cliques connecting *box shape*, *rectangular pocket*, and *through hole* correspond to machining templates frequently seen in prismatic parts, while another community might link *axial gear*, *shaft*, and *keyway*. At higher levels, modularity-based clustering over the category graph yields the thematic groupings visualized in the first image, where related subtrees (e.g., gear systems, bent profiles, and multi-angled structures) are summarized as coherent “families” of shapes. These mined structures directly inform both dataset balancing and the design of tag suggestions for new models.

## F. GPT-5, Gemini, and Human Evaluation.

In continuation of *Section 5* of the main matter, the Fig. 10 describes how a multi-stage workflow was designed to measure the quality of *Face-Type*, *Face-ID*, *Boundary-Type*, and *Boundary-ID* annotations on both 3D scans and their corresponding B-Rep visualizations. As illustrated in the evaluation diagram, the randomly selected 10K samples are first divided into multiple “Eval Batches”, each containing 10 CAD models. For every batch, the 3D scans were color-mapped using the BRep entity feature (see the color map in the teaser figure of the main matter). Thereafter, a corresponding BRep model is also visualized using OpenCASCADE, where the geometric entities are color-mapped to serve as ground truth. Automatic quick snapshots are captured when the CAD models and 3D Scans are collectively rotated to other views. These stacked images are passed to Gemini, GPT-5 to collect the annotation quality scores. The human evaluators also submit their scores in parallel. These scores are aggregated into structured matrices—one for each type of BRep entity labels on the right side of Fig. 10. To avoid redundancy, the other similar matrices for sketches and boundaries are not illustrated. However, we have conducted a similar evaluation for all the boundary, corner, and face-related BRep entities.

### F.1. Chunk-wise Evaluation of Model

We have also unrolled the chunk-wise (0–100) recall and precision measurements for the boundary and junction

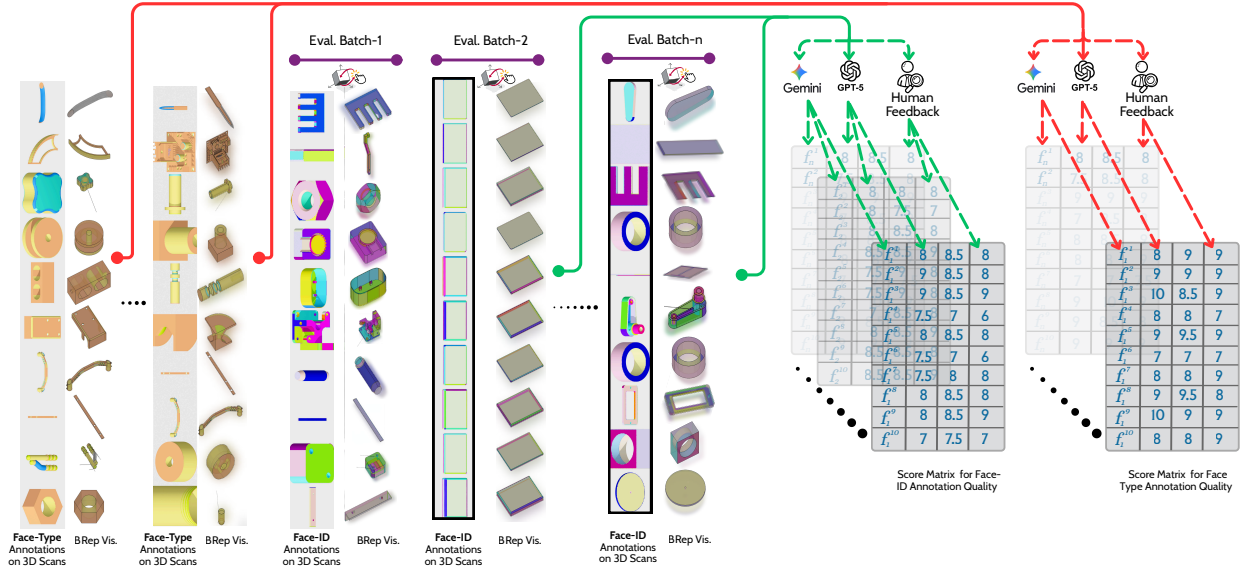


Figure 10. This figure visually describes how evaluation and scoring mechanisms from GPT-5, Gemini, and the Human feedback-based evaluation process for different types of annotations on 10K randomly selected samples.

tasks in Tab. 9. The green colored region, *i.e.*, chunks 70–99, contains 3D scans of a very high-resolution (16x upsampled version of ABC meshes). Therefore, the recall-precision for those chunks is consistently strong. These unrolled results complement the average metrics reported in the main paper. The Fig. 11 illustrated very high-quality boundary and corner detection on a randomly downloaded 3D scan file from the online GrabCAD (<https://grabcad.com/library>) library

## G. More Examples of Caption and Tags

Figs. 13 to 15 illustrates many examples of CAD captions and tags fetched randomly from our **A2Z**. The example captions and tags reveal a *geometry-first* reasoning style: each description starts by carefully characterizing observable shapes (cylinders, plates, frames, blades) and spatial relations (radial, concentric, open-frame), and only then moves to *functional hypotheses* such as cooling, support, or grip. Across both mechanical and decorative objects, the text consistently integrates *local features* (holes, flanges, chamfers, cut-outs) with *global structure* (symmetry, layering, pose) to justify why a part might behave as a fan housing, a probe, a bracket-like stand, or a stylized human figure. The sets of tags act as compact *multi-axis descriptors*, jointly encoding category (e.g., component vs. figurine), function (cooling, fastening, display), dominant geometry (cylindrical body, radial blades, open frame), and likely application domain (industrial machinery, ventilation, artistic display). Together, these captions and tags show how language can remain tightly grounded in CAD evidence while still offering informative, searchable abstractions

that bridge *shape, function, and use context*.

## H. More Examples of Electronic Enclosures

The Fig. 16 and Fig. 17 demonstrate samples that were randomly drawn from our newly added CAD models in **A2Z**, consisting of charging ports, usb-a/b/c type ports, and other socket-type enclosures. The present CAD market for electronic equipment is larger than that for mechanical engineering. The newly added CAD models and results from our foundational model of boundary and junction detection will be highly effective in standardizing the BRep entities of such complex CAD models. Unlike the charging port design data, where the complexity of CAD models is greater in terms of the topology of the folding faces/boundaries, the Fig. 18 illustrates a different challenge regarding the geometric continuity of the BRep faces/boundaries around the corner region. This type of data annotation and our foundational model for parsing the BRep entities are close to industrial settings for accurate CAD reconstruction.

## I. Examples of Annotations and Predictions

In Fig. 19 we add more examples of our rich multi-modal annotations on 3D scans and sketches. The color coding is shown in Fig. 3 of the main matter.

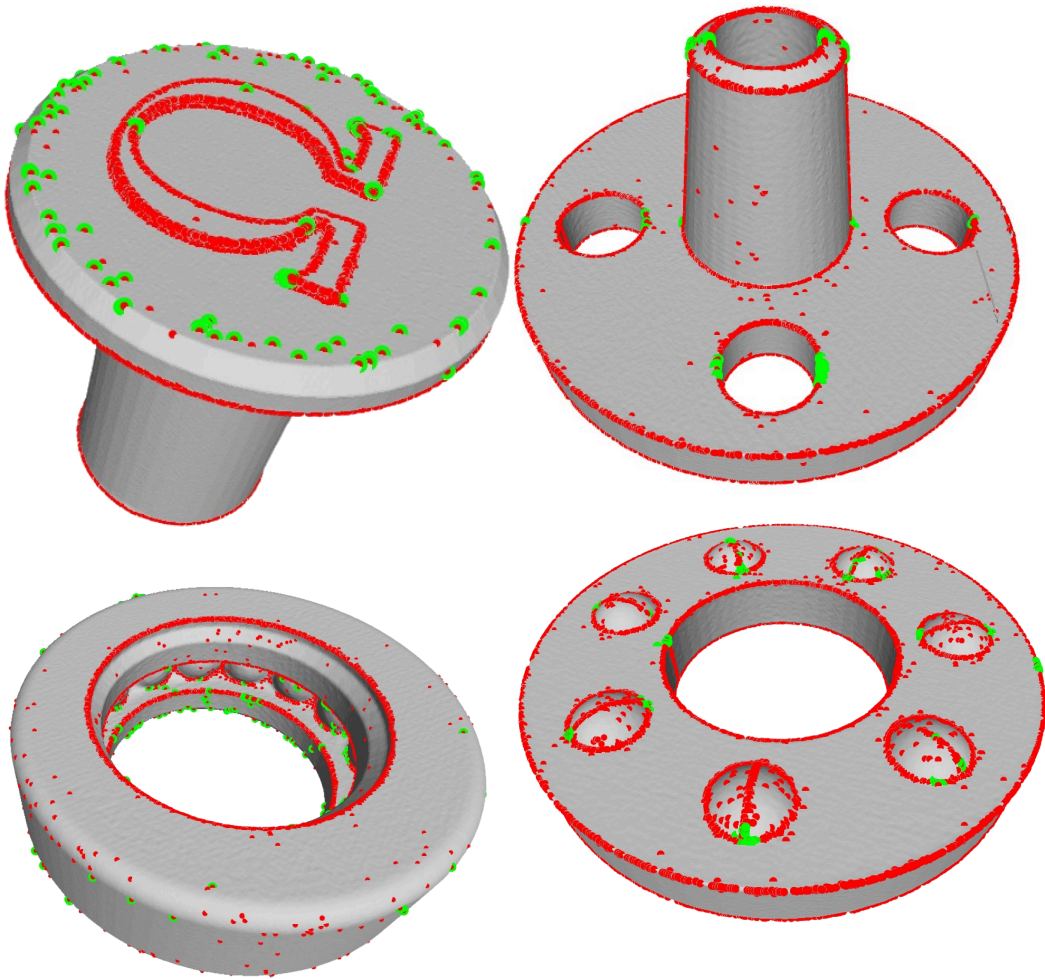


Figure 11. Boundary and Corner detection on randomly selected real-world 3D scan data from the Grab-CAD repository.



Figure 12. Visual comparison between CC3D [7] CAD models, its real scan pairs, and **synthesized scans from CAD (ours)**

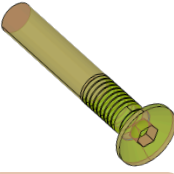
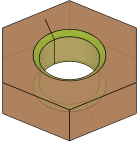
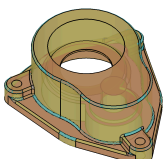
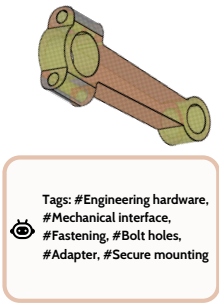
 <p>Tags: #Bolt, #Screw, #ThreadedShaft, #WasherSeat, #CylindricalBody, #HexagonalHead</p>	<p>A cylindrical fastener, a bolt or a screw, characterized by a threaded shaft and a head. The shaft is a long, cylindrical body with evenly spaced threads along half of its length. The head is hexagonal, a typical design for a socket head cap screw, allowing for the application of torque. The head also features a recessed area, possibly for a washer or a nut, and a small rectangular feature that could be a locking mechanism or a washer seat. The transition between the shaft and the head is smooth, with a fillet radius, ensuring a secure and rounded connection. The overall structure is symmetrical along the central axis, with the head and shaft maintaining a consistent diameter throughout.</p>	 <p>Tags: #Hexagonal Adapter, #Mechanical Coupling, #Mechanical Assembly, #Chamfered Edges, #Central Cutout, #Cylindrical Bore,</p>	<p>A mechanical component with a hexagonal outer shape and a cylindrical inner bore. The hexagonal shape is concentric with the cylindrical bore, suggesting it is designed to fit within or around another cylindrical part. The component has a central circular cutout, for accommodating a shaft or rod. The outer hexagonal surface has a slight chamfer or fillet at the edges, which may serve to ease assembly or reduce stress concentrations. The symmetry is evident across all views, indicating uniformity in design. This geometry suggests it could be used as a coupling or adapter in mechanical systems, possibly for aligning or securing cylindrical components in machinery.</p>
 <p>Tags: #Smartphone case, #Protective casing, #Fillet edges, #Camera cutout, #Charging port cutout, #Speaker cutout</p>	<p>This is a protective case for a smartphone, given its rectangular shape and the presence of cutouts for the camera, flash, and speaker. The case is designed to fit snugly around the device, featuring a smooth, rounded edge that provides a comfortable grip. The primary structure consists of a flat base and a top cover, both of which are connected by a series of vertical walls. The case features a series of cutouts for the camera, flash, and speaker, as well as a small rectangular cutout near the bottom, for a charging port or microphone. The edges of the case are reinforced with thicker material, providing additional protection and structural integrity. The overall design is symmetrical, with identical cutouts and structural elements on both the front and back of the case.</p>	 <p>Tags: #Coupling, #Mechanical Component, #Flanged Shaft, #Radial Slots, #Cylindrical Shaft, #Rotational Alignment, #Rotational Coupling, #Alignment Mechanism</p>	<p>A mechanical coupling component, characterized by its cylindrical shaft with flanged ends. The primary geometry consists of a central cylindrical shaft with two flanged sections at each end, each featuring a series of radial slots. These slots are for keyways or alignment purposes. The flanges have central holes, presumably for fastening or alignment with other components. The radial slots and central holes suggest a design intended for secure attachment and rotational alignment. The symmetry along the axial direction indicates that the component is designed for balanced rotational motion. This type of component is commonly used in machinery to connect two shafts securely, ensuring synchronized rotational movement.</p>
 <p>Tags: #Architectural Model, #Residential Building, #Gabled Roof, #Chimney, #Front Door, #Windows, #Railings</p>	<p>A detailed architectural CAD model of a residential building, characterized by its rectangular prism base and gabled roof. The structure includes multiple windows, a front door with a small porch, and a chimney. The roof has a slight overhang, and there are external staircases leading to an upper entrance. The building exhibits bilateral symmetry along its longitudinal axis, with evenly spaced windows and doors. The presence of balconies and railings suggests additional access points. This model is used for architectural visualization or urban planning.</p>	 <p>Tags: #Coupling, #Mounting Holes, #Automotive Use, #Mechanical Component, #Transmission System, #Flanged Design, #Engineering Hardware, #Industrial Machinery</p>	<p>A mechanical coupling component, characterized by a central circular opening surrounded by two smaller circular holes on either side. The geometry includes a cylindrical central section with a larger diameter, flanked by two symmetrical, elongated arms. Each arm has a circular hole near its end, for mounting purposes. The component exhibits radial symmetry around the central axis, with smooth transitions between the cylindrical sections and the arms. The presence of multiple holes suggests it is designed for secure attachment to other components, possibly in a rotational or transmission system. The overall design indicates it could be used in machinery requiring precise alignment and secure connections, such as in automotive or industrial equipment.</p>
 <p>Tags: #Coupling, #Flanged, #Bolt holes, #Cylindrical body, #Protrusion #Industrial machinery, #Shaft</p>	<p>A mechanical coupling component, characterized by a cylindrical central section with a flanged base. The primary geometry consists of a concentric cylindrical body with a larger flange at one end, featuring multiple bolt holes for secure mounting. The flange has a rectangular shape with rounded corners and four evenly spaced holes, for fastening to another component. The cylindrical section has a smooth outer surface with a slight radial protrusion near the flange, possibly for alignment or additional mechanical support. This component is used in industrial machinery to connect two shafts securely, allowing torque transmission while accommodating slight misalignments.</p>	 <p>Tags: #Audio Equipment, #Speaker Housing, #Component Mounting, #Protective Housing, #Cylindrical Protrusions, #Ventilation Holes</p>	<p>A mechanical enclosure for audio equipment, cylindrical protrusions at each end. The front face features a rounded rectangular cutout with two smaller circular cutouts adjacent to it, for a control panel or interface. This component could be used in audio equipment, such as a speaker housing.</p>
 <p>Tags: #Booth, #Miniature structure, #Vertical panels, #Peaked roof, #Circular finial, #Architectural model</p>	<p>A box-like structure with a pitched roof, resembling a miniature booth or kiosk. It features a rectangular base with vertical panels and a peaked roof with a circular finial at the apex. The structure has symmetrical sides with rectangular cutouts or windows similar to a cadbury pattern, and the front includes a door with a visible handle. The roof is slightly overhanging, providing a small eave around the perimeter. The design suggests a standalone unit, possibly for informational or security purposes. The overall symmetry and geometric simplicity indicate it could be used in architectural models or as a decorative element in landscaping.</p>	 <p>Tags: #Laptop, #Clamshell Design, #Keyboard Layout, #Touchpad, #Hinged Lid, #Electronic Housing, #Portable Device, #Display Screen, #Computing Device</p>	<p>A laptop CAD model, characterized by its rectangular prism shape with a hinged lid. The primary geometric forms include a flat rectangular base with a keyboard layout and a screen on the lid. The hinge mechanism allows the lid to open and close, indicating a clamshell design. Key features include flat chiclet keys without dedicated number pads, a touchpad, and a rectangular screen area. The laptop has symmetrical sides with visible cutouts for ports or ventilation. The overall design suggests a portable electronic device, used for computing tasks.</p>

Figure 13. Visual elaboration of the textual captions on more complex CAD models.



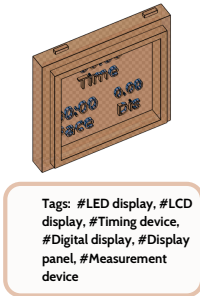
Tags: #Protective casing, #Enclosure, #Connectivity ports, #Electronic equipment, #Branding markings

Handheld electronics enclosure resembling a smartphone front housing. The part is a thin-walled rectangular prism with a large recessed display pocket, rounded corners, and a perimeter step/lip for a mating cover or glass. Apertures include a long speaker/vent slot, an around home/feature slot, small circular sensor/camera holes, and side cutouts for buttons or connectors. Surfaces are predominantly planar, with corner fillets and light chamfers. Features are symmetric about the mid-plane and centered along the long axis. Typically used as a mobile device bezel/frame, it provides protection, alignment, and interface openings for user input/output and components.



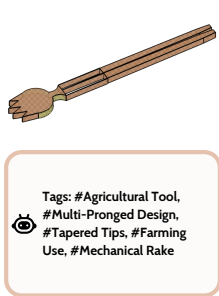
Tags: #Engineering hardware, #Mechanical interface, #Fastening, #Bolt holes, #Adapter, #Secure mounting

A mechanical coupling or adapter, characterized by a cylindrical body with flanged ends. The primary geometry consists of a central cylindrical shaft with two flanged sections at each end, each featuring multiple bolt holes for secure mounting. The flanges are symmetrical and have a circular arrangement of holes, for fastening to other components. The spatial relationship between the flanges and the central shaft indicates that this part is intended to join two cylindrical components, in a mechanical or industrial setting. The presence of multiple bolt holes suggests it is designed for a secure, fixed connection, used in machinery or structural assemblies.



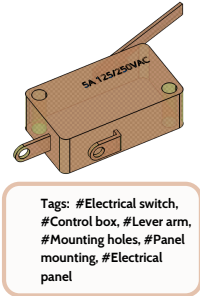
Tags: #LED display, #LCD display, #Timing device, #Digital display, #Display panel, #Measurement device

A rectangular electronic housing or enclosure, characterized by its box-like structure with a front panel featuring digital displays. The primary geometric form is a rectangular prism with a flat front face. The front panel includes cutouts for digital displays showing "Time", "Pace" and "Dist" suggesting it is designed to house electronic components such as LED or LCD displays. The enclosure has mounting holes on the top and bottom edges, indicating it is meant to be secured to another surface. ... This housing is used in timing or measurement devices, for sports or fitness equipment, where tracking time, pace, and distance is essential.



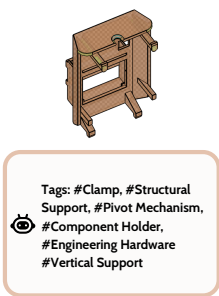
Tags: #Agricultural Tool, #Multi-Pronged Design, #Tapered Tips, #Farming Use, #Mechanical Rake

A multi-pronged tool, a rake or similar agricultural implement. It consists of a long, cylindrical handle with multiple parallel prongs at one end, which are evenly spaced and taper slightly towards the tips. The handle is segmented, suggesting flexibility or ease of assembly. The prongs are connected to the handle via a series of rectangular cutouts, allowing for a secure yet flexible attachment. The geometry includes a cylindrical shaft with radial symmetry, transitioning into a flared, multi-fingered end. The design suggests a function related to gathering or raking materials, with the prongs providing a wide surface area for efficient collection.



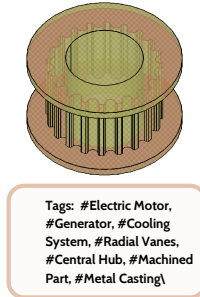
Tags: #Electrical switch, #Control box, #Lever arm, #Mounting holes, #Panel mounting, #Electrical panel

A mechanical housing or enclosure, characterized by a rectangular prism with a flat top surface. It features four mounting holes at the corners, for securing it to another component. The presence of additional holes and cutouts indicates points for electrical connections or cable entry. The labeling "5A 125/250VAC" implies electrical specifications, hinting at its use in electrical control systems. The overall geometry and features suggest it could be part of an electrical switch or control box, used in industrial or electrical applications for housing and protecting internal components while allowing manual interaction.



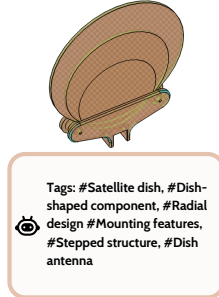
Tags: #Clamp, #Structural Support, #Pivot Mechanism, #Component Holder, #Engineering Hardware, #Vertical Support

A mechanical fixture or clamp, characterized by a rectangular base with a vertical support structure and a horizontal top plate. The base has two protruding legs with holes, for mounting purposes. The vertical support includes a rectangular cutout, for alignment or securing another component. The top plate has a central hole, which may serve as a pivot or attachment point. The design includes several fillets and chamfers, indicating considerations for stress distribution and ease of assembly. The overall symmetry and spatial arrangement suggest it is designed to hold or secure another part in place, in a manufacturing or assembly setting.



Tags: #Electric Motor, #Generator, #Cooling System, #Radial Vanes, #Central Hub, #Machined Part, #Metal Casting

A mechanical component with a cylindrical base and a central hub, featuring multiple radial fins or vanes. The primary geometry consists of concentric cylindrical sections with a central circular cutout. The outer ring has a series of evenly spaced, vertical fins extending radially inward, which serve to dissipate heat or provide structural support. The inner section has a smaller cylindrical protrusion with similar radial features. The symmetrical arrangement and the presence of these fins suggest it could be part of a rotor or a heat sink. The component's design indicates it might be used in applications requiring thermal management or rotational stability, such as in electric motors, generators, or cooling systems.



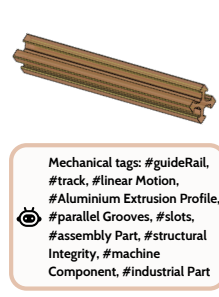
Tags: #Satellite dish, #Dish-shaped component, #Radial design, #Mounting features, #Stepped structure, #Dish antenna

A Tilt-adjustable circular panel, featuring a large, circular, dish-like structure supported by a central cylindrical shaft. The primary geometric form is a concave dish with a flat base, which is mounted on a vertical shaft. The dish has a transverse pin/holes that create a pivot about the panel's axis. The base of the dish includes several cylindrical protrusions, for mounting or alignment purposes. The shaft has a series of rectangular blocks and cylindrical elements, indicating points of attachment or support. The overall symmetry is radial with the dish centered on the shaft. This design suggests a component that might be used in applications requiring rotational movement or support, such as in satellite dishes, radar systems, or industrial machinery.



Tags: #Brush Assembly, #Circular Bristles, #Surface Cleaning, #Contact Mechanism, #Rotational Symmetry

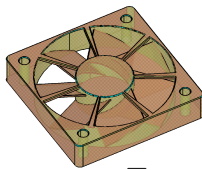
A cylindrical mechanical component with a brush-like end, a brush holder, or a similar device. The primary geometry consists of a long cylindrical body with a smaller cylindrical section at one end, which transitions into a brush assembly. The brush end features bristles arranged in a circular pattern, suggesting a cleaning or contact function. The component exhibits axial symmetry, with the brush assembly positioned at one end and the cylindrical body extending uniformly. The presence of the brush and the cylindrical form suggests it could be used in applications requiring surface contact or cleaning, such as in industrial machinery or automotive systems.



Mechanical tags: #guideRail, #track, #linear Motion, #Aluminium Extrusion Profile, #parallel Grooves, #slots, #assembly Part, #structural Integrity, #machine Component, #Industrial Part

The CAD model of an Aluminium Extrusion Profile, a part of a machine or system that requires precise alignment and structural integrity. A rectangular prism with a series of parallel grooves and slots along its length, a guide rail-track for linear motion. The symmetrical arrangement of the grooves and slots, along with the precise alignment of the edges, indicates that this part is designed to fit into a larger assembly where it will guide or support moving parts. The flat faces and precise edges suggest that the part is manufactured using CNC machining techniques, and it lacks cylindrical bosses or cutouts. It is a component that is to be mounted or integrated into a larger structure rather than being a standalone part.

Figure 14. Visual elaboration of the textual captions on more complex CAD models



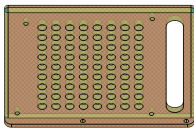
Tags: #Cooling system, #Radial blades, #Axial flow, #Radial fan, #Blade assembly, #Ventilation component, #Airflow

A mechanical component with a central hub and multiple radial blades extending outward, enclosed within a square frame. The central hub is circular and concentric with the radial blades, which are evenly spaced and symmetrically arranged. The square frame has four mounting holes at each corner, suggesting it is designed for secure attachment to another surface. The component exhibits a combination of cylindrical and prismatic forms, with the blades creating a fan-like structure. The overall symmetry and the presence of mounting holes indicate it is used for ventilation or cooling purposes, as a fan housing or blower assembly.



Tags: #Trophy, #Award Cup, #Grip Feature, #Ceremonial Use, #Decorative Item, #Competition Award, #Angular Handles, #Flared Top, #Cylindrical Body, #Industrial Design

A trophy or an award cup, characterized by its symmetrical three-dimensional geometry. It consists of a cylindrical body with a flared top, supported by a rectangular base. The cylindrical body has two handles extending radially from the upper section, which are angular and slightly curved. The base is square with a central circular platform that supports the cylindrical body. The spatial relationship between the components is concentric, with the cylindrical body centered on the base. The handles provide a grip feature, while the cylindrical body and base are connected seamlessly, suggesting a monolithic structure. This design is typical for decorative or ceremonial objects, used in events or competitions for recognition purposes.



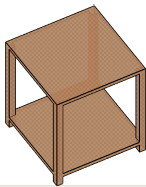
Tags: #Heat sink, #Metal plate, #Ventilation, #Circular holes, #Grid pattern, #Uniform distribution, #Plate

A rectangular plate with a series of circular holes arranged in a 4x8 grid pattern. The plate features a rectangular cutout on one side for mounting or alignment purposes. The holes are evenly spaced and cover most of the plate's surface, which resembles an optical breadboard. The edges of the plate are smooth, with no visible chamfers or fillets, indicating a straightforward manufacturing process. The symmetry of the hole pattern and the rectangular cutout suggests that this part could be used in applications requiring uniform distribution of forces or airflow. The overall geometry and features imply that it might serve as a mounting plate or a heat sink in industrial machinery.



Tags: #Floral Motif, #Display Item, #Decorative Box, #Leaf Pattern, #Ornamental Artwork, #Wood-Like Material, #Handcrafted Appearance, #Artistic Embellishment

A rectangular box with intricate surface engravings. It has a symmetrical design with a central ornamental pattern featuring floral and leaf motifs. The box has a flat top surface with detailed embossing, and the sides are slightly raised, forming a shallow rectangular prism. The corners are rounded, and there are no visible mounting features, holes, or cutouts. The overall symmetry and decorative nature suggest it could be a decorative box or container, used for aesthetic purposes or as a small storage unit.



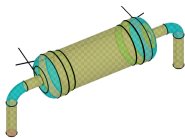
Tags: #Shelving Unit, #Structural Support, #Support Frame, #Open Frame, #Display Stand, #Industrial Furniture

A two-tiered open-frame structure with a rectangular base and an elevated rectangular platform. The primary geometric forms include rectangular prisms, with the upper and lower tiers aligned axially. The design features clean, sharp edges with no visible fillets or chamfers. The structure lacks any mounting holes or cutouts, suggesting it may serve as a standalone unit or a part of a larger assembly. The symmetrical arrangement and open design indicate potential use as a shelving unit or a support frame. The simplicity and open nature suggest it could be used in storage solutions or as a display stand in industrial or office settings.



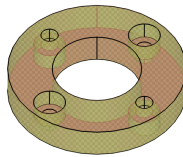
Tags: #Human Figure, #Stylized Representation, #Ballet Pose, #Human Movement, #Figure Sculpture, #Artistic Model, #Dance Study, #Pose Variation

A stylized representation of a human figure in various ballet poses, rather than a mechanical component. The geometry consists of a central body with limbs extended in different directions, suggesting movement and flexibility. The figure has a rounded head, a torso with a flared skirt-like structure, and elongated limbs. The limbs are positioned in various ballet stances, indicating dynamic poses. There are no visible mounting features, holes, or cutouts, and the surface transitions are smooth with no distinct fillets or chamfers. The overall symmetry is bilateral, with each pose reflecting a mirrored counterpart. While not a mechanical part, this figure could be used in artistic or educational applications, as a model for studying human movement or dance.



Tags: #90-Degree Pipe Bends, #Piping, #Pipe Fitting, #Flanged Adapter, #Cylindrical Component, #Gas Transfer System

A cylindrical flow-through canister with pipe connections. It features a central axis-symmetric cylinder with stepped collars/weld bands near each end, each end pipe with a smooth 90-degree elbow bend. The body is adorned with several bands, for reinforcement or attachment purposes. The component exhibits axial symmetry, with the bands evenly spaced around the circumference. The flanges at the ends suggest it is designed for secure mounting or connection to other components. The presence of these flanges and the overall cylindrical shape indicates that it could be used in fluid or gas transfer systems, as a coupling or adapter, and with constant-ID tubing for uninterrupted flow.



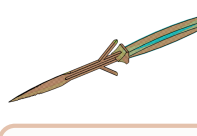
Tags: #Flanged Coupling, #Spacer, #Mounting Holes, #Industrial Machinery, #Mechanical Assembly, #Central Bore, #Fastening Feature, #Radial Holes, #Shaft Alignment

A circular mechanical component with a central hole and multiple peripheral features. It is primarily cylindrical with a concentric arrangement of holes around its perimeter. The component has a central circular cutout, surrounded by a thicker ring. There are eight evenly spaced holes around the outer ring, each with a smaller concentric hole, for mounting or fastening purposes. The inner and outer edges of the component have slight chamfers, and the overall design suggests symmetry and balance. This geometry is typical of a flanged coupling or a spacer used in mechanical assemblies to connect shafts or provide spacing between components. The mounting holes indicate it is designed to be secured in place, in machinery or industrial equipment.



Tags: #Probe, #Stylus, #3D Scanning, #Conical Tip, #Measurement Tool, #Contact Measurement, #Precision Component

A cylindrical mechanical component with a tapered tip, a type of probe or stylus. The primary geometry consists of a long, straight cylindrical body with a smaller diameter section near the top, transitioning into a conical tip. The cylindrical body has a uniform diameter, while the conical tip is sharply pointed, suggesting precision in its design. The symmetry is axial, with the conical tip aligned along the central axis of the cylinder. This geometry suggests that the component could be used in applications requiring precise contact or measurement, such as in sensors, probes, or styluses for 3D scanning.



Tags: #Spear, #Javelin, #Pointed tip, #Grip section, #Aerodynamic shape, #Parallel prongs, #Throwing spear, #Combat tool, #Crossguard, #Pointed projectile

A spear or javelin, characterized by a long slender shaft with a pointed tip. The shaft is cylindrical with a consistent diameter, transitioning into a tapered point at one end. The other end features a crossguard, which is perpendicular to the shaft, providing balance and protection. The crossguard is composed of two parallel prongs, symmetrically aligned. The spear also includes a grip section, slightly thicker than the main shaft, designed for secure handling. The overall design suggests a focus on aerodynamic efficiency and stability during flight, with the crossguard enhancing control and safety.

Figure 15. Visual elaboration of the textual captions on more complex CAD models

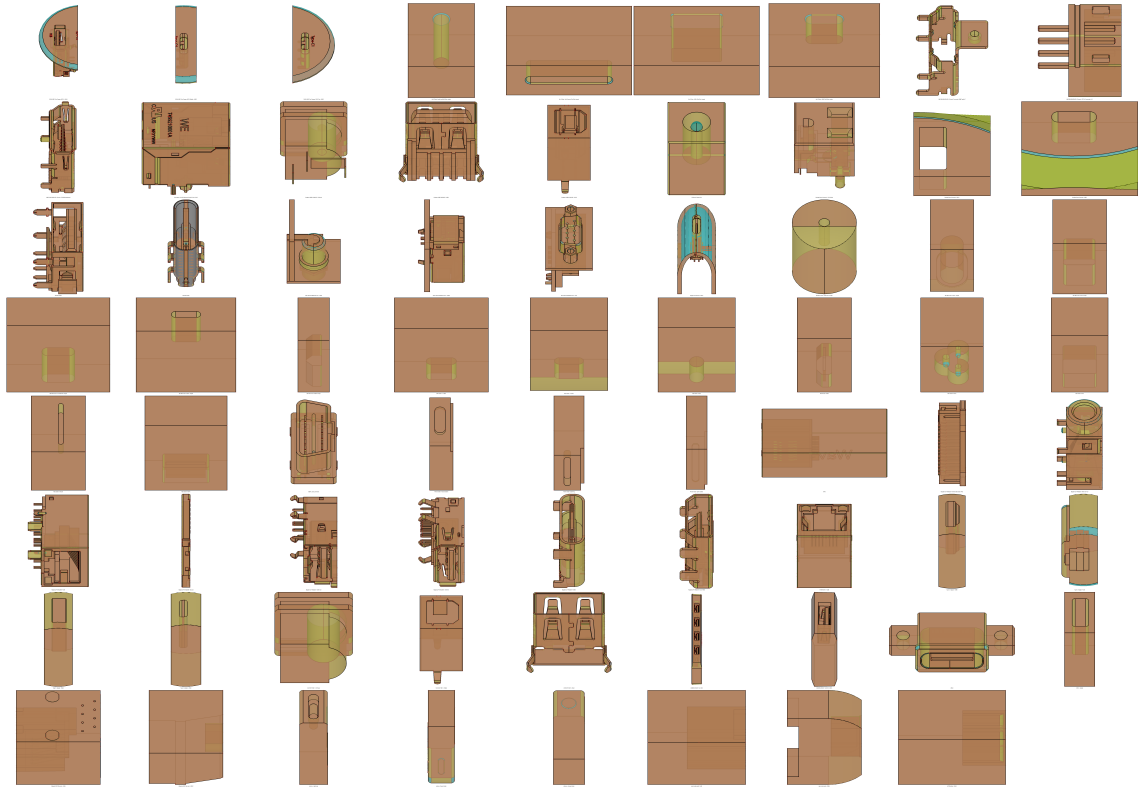


Figure 16. Visuals of some randomly selected CAD models of charging ports under **A2Z**. Color codes define face-Types.

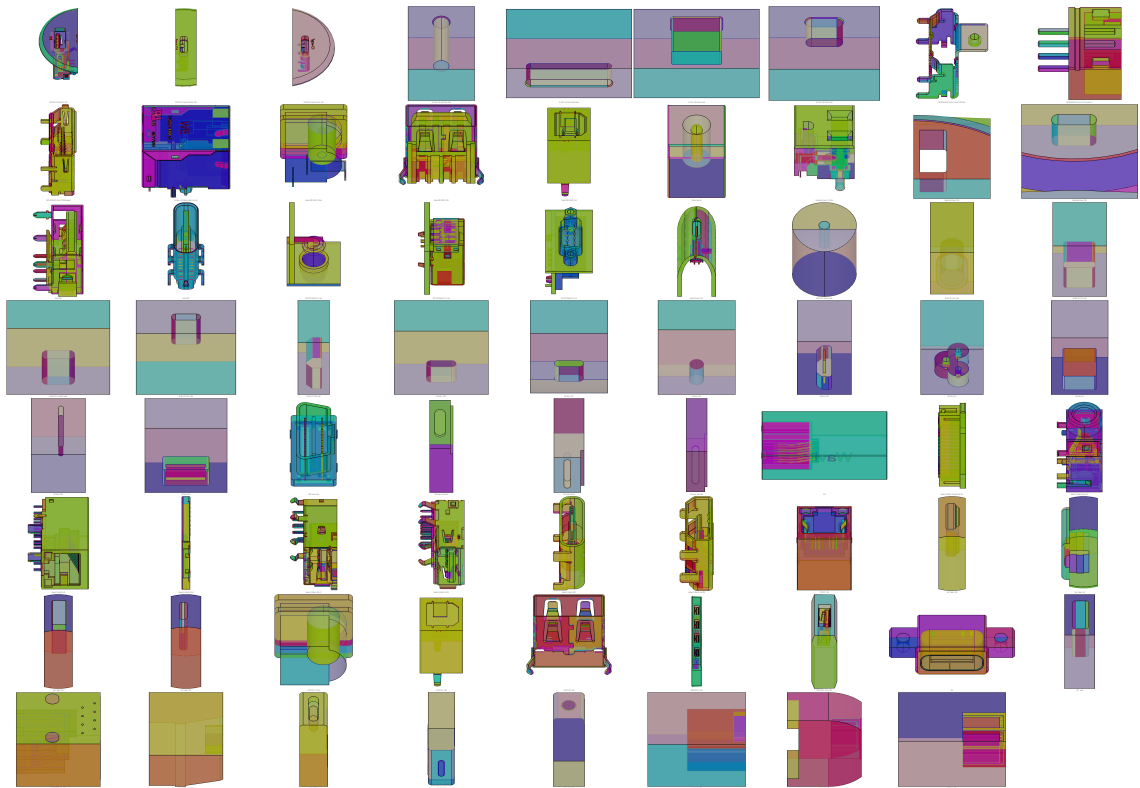


Figure 17. Visuals of same CAD models of charging ports under **A2Z** where color codes define face-IDs.

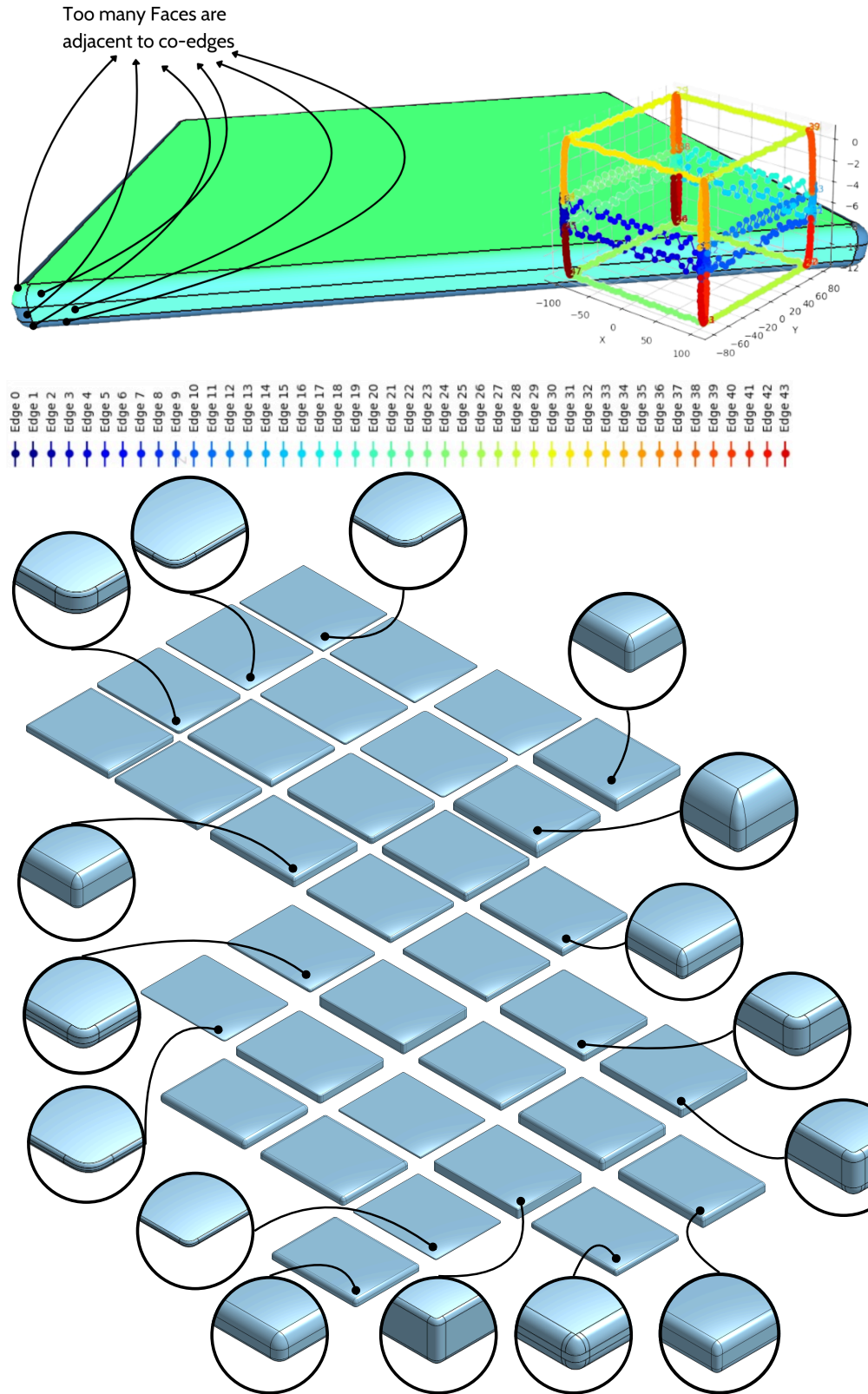


Figure 18. Visuals of some randomly selected samples of CAD models for Tablet type enclosures (from Approx. 20K Electronic enclosure models) with varying corner geometry and topology (*at bottom*). A closer look at the BRep faces, edges, and vertices near the corner parts (*on top*) shows how many faces are adjacent to each edge.

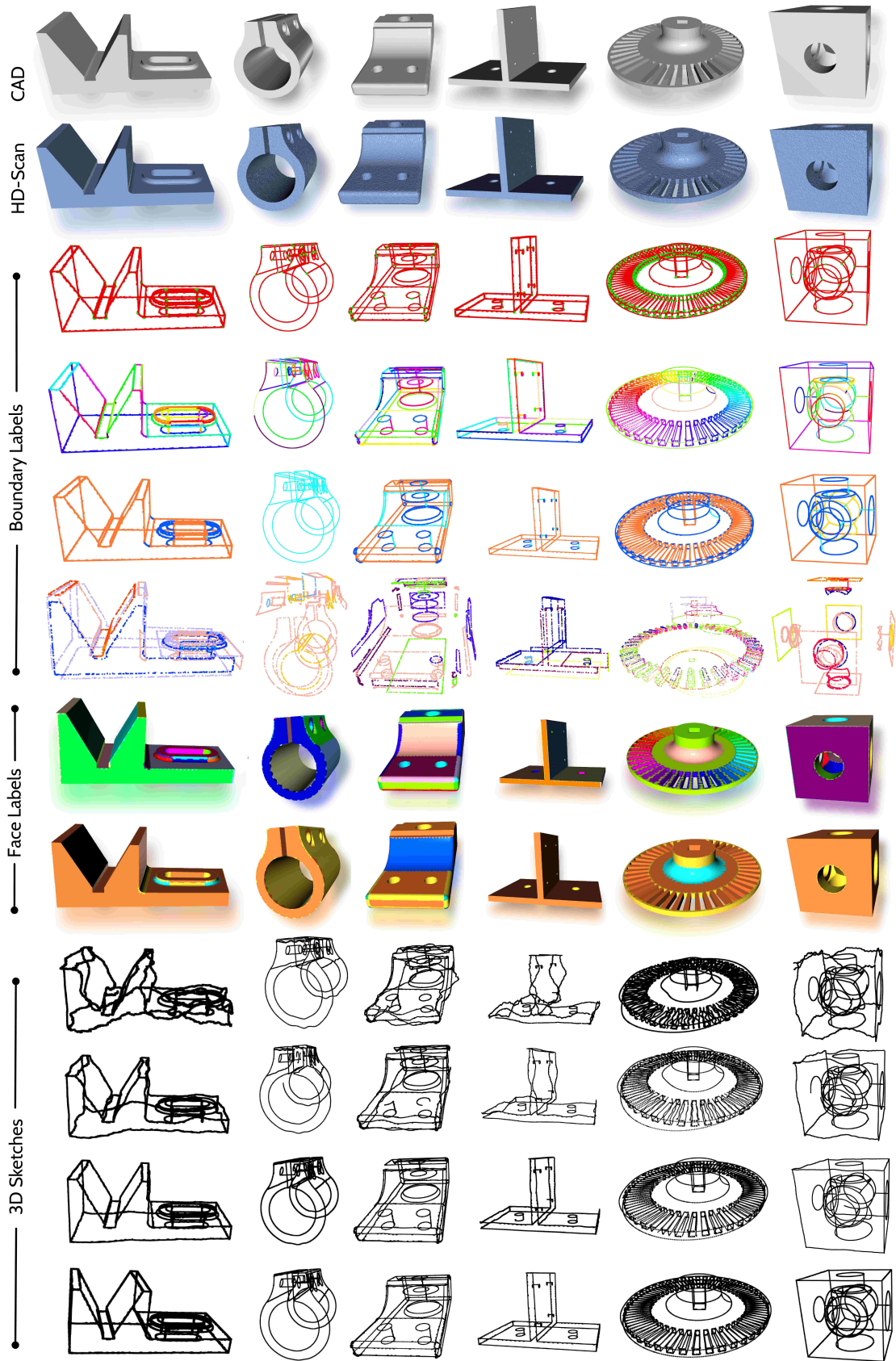


Figure 19. More visual examples of BRep Annotations for reverse engineering from 3D scans/sketches.

Chunk	Boundary		Junction		Chunk	Boundary		Junction	
	Recall	Precision	Recall	Precision		Recall	Precision	Recall	Precision
0	0.972	0.885	0.690	0.740	50	0.974	0.888	0.642	0.728
1	0.972	0.905	0.710	0.774	51	0.980	0.900	0.670	0.723
2	0.980	0.883	0.681	0.703	52	0.967	0.885	0.665	0.739
3	0.977	0.883	0.688	0.739	53	0.971	0.882	0.675	0.726
4	0.964	0.841	0.698	0.701	54	0.965	0.876	0.639	0.734
5	0.977	0.877	0.688	0.765	55	0.963	0.895	0.668	0.759
6	0.972	0.889	0.673	0.764	56	0.950	0.884	0.629	0.726
7	0.958	0.851	0.690	0.791	57	0.966	0.886	0.686	0.749
8	0.961	0.879	0.682	0.708	58	0.970	0.888	0.673	0.743
9	0.972	0.877	0.682	0.731	59	0.970	0.885	0.645	0.748
10	0.982	0.878	0.692	0.780	60	0.965	0.885	0.641	0.756
11	0.973	0.878	0.689	0.710	61	0.975	0.876	0.657	0.742
12	0.965	0.868	0.698	0.711	62	0.979	0.887	0.668	0.720
13	0.980	0.895	0.678	0.737	63	0.972	0.882	0.674	0.743
14	0.970	0.900	0.696	0.736	64	0.967	0.867	0.641	0.676
15	0.974	0.890	0.683	0.747	65	0.967	0.911	0.682	0.760
16	0.939	0.876	0.703	0.740	66	0.965	0.885	0.640	0.716
17	0.974	0.864	0.682	0.680	67	0.963	0.878	0.637	0.757
18	0.958	0.874	0.674	0.778	68	0.978	0.888	0.684	0.748
19	0.973	0.886	0.679	0.745	69	0.974	0.894	0.657	0.763
20	0.959	0.870	0.702	0.755	70	0.981	0.909	0.781	0.897
21	0.971	0.881	0.688	0.707	71	0.978	0.892	0.775	0.917
22	0.979	0.886	0.680	0.765	72	0.980	0.890	0.777	0.931
23	0.976	0.891	0.678	0.747	73	0.987	0.909	0.782	0.928
24	0.979	0.898	0.683	0.771	74	0.983	0.900	0.776	0.902
25	0.978	0.876	0.681	0.748	75	0.983	0.899	0.772	0.893
26	0.963	0.880	0.688	0.736	76	0.985	0.896	0.777	0.938
27	0.963	0.857	0.695	0.739	77	0.986	0.884	0.783	0.909
28	0.956	0.870	0.695	0.692	78	0.986	0.913	0.775	0.873
29	0.970	0.887	0.681	0.763	79	0.980	0.895	0.777	0.941
30	0.967	0.891	0.695	0.799	80	0.985	0.900	0.784	0.940
31	0.970	0.885	0.651	0.744	81	0.981	0.893	0.775	0.917
32	0.972	0.896	0.658	0.777	82	0.981	0.896	0.741	0.917
33	0.964	0.848	0.656	0.715	83	0.987	0.901	0.782	0.932
34	0.979	0.901	0.658	0.714	84	0.984	0.905	0.779	0.844
35	0.965	0.873	0.658	0.726	85	0.985	0.917	0.767	0.869
36	0.980	0.895	0.651	0.714	86	0.981	0.883	0.744	0.929
37	0.958	0.852	0.648	0.794	87	0.983	0.895	0.740	0.912
38	0.968	0.871	0.621	0.759	88	0.984	0.905	0.742	0.895
39	0.975	0.872	0.674	0.724	89	0.986	0.895	0.740	0.872
40	0.978	0.903	0.660	0.731	90	0.977	0.894	0.748	0.913
41	0.974	0.866	0.662	0.756	91	0.981	0.896	0.748	0.931
42	0.967	0.886	0.659	0.731	92	0.984	0.885	0.752	0.915
43	0.964	0.874	0.656	0.700	93	0.984	0.891	0.742	0.899
44	0.948	0.861	0.653	0.751	94	0.983	0.902	0.742	0.934
45	0.972	0.872	0.659	0.727	95	0.986	0.903	0.741	0.915
46	0.966	0.888	0.673	0.766	96	0.982	0.877	0.745	0.912
47	0.976	0.894	0.638	0.726	97	0.983	0.886	0.778	0.920
48	0.979	0.881	0.639	0.741	98	0.982	0.884	0.779	0.924
49	0.961	0.864	0.635	0.721	99	0.977	0.870	0.781	0.893

Table 9. Precision-recall measures for all 100 chunks of **A2Z** using our foundation model.